THE PLASMA ENVIRONMENT OF NEPTUNE

J. D. RICHARDSON, J. W. BELCHER, and A. SZABO
Massachusetts Institute of Technology

and

R. L. McNUTT, JR.
Applied Physics Laboratory

This chapter describes the Voyager 2 plasma observations near Neptune. We describe features in the order they were observed by Voyager. The bow shock was nearly perpendicular at the time of the encounter, with a Mach number of 4.5 and an outward velocity of about 15 km s^{-1}. Voyager 2 entered the magnetosphere of Neptune through the cusp region; the magnetopause crossing is a rotational discontinuity, indicating that a dynamic mantle region is formed. The magnetospheric plasma is created from neutral atoms which escape from Triton's atmosphere and are ionized in the magnetosphere. Both protons and heavy ions, probably nitrogen, are detected. The plasma density is very low; the peak density of 2 cm^{-3} occurs near closest approach to Neptune. The plasma temperature increases nearly adiabatically as the planet is approached. Both the density and temperature profiles are consistent with inward motion of plasma from a Triton source. Losses of both plasma and energy occur near Neptune; these may be due to precipitation, charge exchange, and/or ring absorption. Estimates of neutral escape from Triton combined with the plasma observations imply neutral densities of the order of 100 cm^{-3}. In the outbound magnetosheath Voyager made the first detection of the penetration of the plasma mantle into the magnetosheath of a planet. Mantle plasma extends through a substantial portion of the magnetosheath at high latitudes. As at all the other magnetized planets, upstream waves are detected in the solar wind when the spacecraft is magnetically connected to the bow shock.

I. INTRODUCTION

The encounter of Voyager 2 with the giant planet Neptune in August of 1989 concluded the initial reconnaissance of the solar system's giant planets. The brief flyby of Neptune produced observations of the sixth planet in the solar system with an intrinsic magnetic field and the fourth giant planet magnetosphere. Like its relative Uranus, Neptune possesses a highly tilted magnetic dipole moment. Neptune's dipole axis is oriented 47° from its rotational axis (Connerney et al. 1991); the corresponding angle for Uranus is 58.6° (Ness et al. 1991). Neptune has a relatively "normal" inclination of its spin axis to the plane of its orbit, 29°, as compared with 98° for Uranus (Allen 1973), so

Neptune's magnetosphere is a unique case and of great value for comparative magnetosphere studies. Neptune's magnetosphere contains an internal source of heavy-ion plasma, its moon Triton, which possesses both an atmosphere and a surprisingly substantial ionosphere (Tyler et al. 1989). Although Triton is located about 14 R_N from Neptune (1 R_N≡24,765 km), matter originating at Triton is observed in the inner magnetosphere. As with every planet so far encountered, Neptune's magnetosphere occupies a unique niche with respect to plasma sources and transport.

We begin with an explanation of some of the more salient ideas of magnetospheric plasma physics used in this review and discuss some of the expectations for Neptune. Next, we give an overview of the encounter data and observational results and discuss the implications for magnetospheric physics at Neptune. In turn, properties of the inbound bow shock, magnetosheath/cusp, magnetosphere, and downstream waves are considered. We end with a comparison of Neptune's magnetosphere with those of the other giant planets in the solar system. Results presented here are primarily based upon observations made by the Plasma Science Experiment (PLS) on Voyager 2, an electrostatic instrument which measures electrons and positive ions in the nominal energy-per-charge range of 10 V to 5950 V (Bridge et al. 1977).

A. Magnetospheric Plasma Physics: A Brief Tutorial

This section reviews some of the basic tenets of magnetospheric physics for the reader not familiar with this field. It is intended to provide a brief glossary of terms and concepts used later in the chapter.

Ions and electrons gyrate around magnetic field lines and also move along field lines. The frequency of these gyrations is called the cyclotron frequency and the radius of the gyrations is called the gyroradius. The speed of these random motions, called the thermal speed, defines a plasma temperature through the relation $kT_i = \frac{1}{2}m_i w_i^2$ where k is Boltzmann's constant, i identifies the particle species, and w is the thermal speed. Rigorously, this identification applies if the particle speeds are distributed with a Maxwellian (Gaussian) distribution. In the collisionless plasmas found in the solar wind and magnetospheres, non-Maxwellian distributions often occur. One method of characterizing these distributions is to use a set of several Maxwellian distributions with different temperatures such that the sum of these thermal distributions approximates the true distribution function of the plasma. Plasma can have different distributions of speeds perpendicular and parallel to the magnetic field direction. If these distributions are the same, then the plasma distribution function is said to be isotropic (in velocity space). If the distributions are different but Maxwellian, then one speaks of a bi-Maxwellian, or anisotropic, distribution with parallel and perpendicular thermal speeds $w_\parallel$ and $w_\perp$ and corresponding temperatures $T_\parallel$ and $T_\perp$.

The guiding center approximation (see, e.g., Northrup 1963) allows us to ignore the gyromotion (except for determining the plasma temperature) and look only at the average location (gyrocenter) of the plasma particles to determine the plasma motion. It is the average motion of the gyrocenter that defines the plasma bulk, or convective, velocity.

Another assumption used is the "frozen-in condition" (see, e.g., Sec. 13.5 of Rossi and Olbert 1970). This states that the plasma and magnetic field move together (a consequence of Faraday's law when applied to typical magnetospheric plasma conditions) and is valid throughout the Neptune region except, perhaps, at the bow shock. One consequence of this condition is that the plasma tends to rotate with the planet, because the planetary magnetic field threads the Neptunian ionosphere (a good conductor) which, in turn, rotates with the planet. Thus the plasma velocity will vary as the distance from the spin axis, as plasma throughout the magnetosphere must completely circle the planet every Neptunian day. Plasma whose angular velocity matches that of the planet is said to be corotating and the velocity this corresponds to is the corotation velocity.

Because plasma remains on the same magnetic field line, the magnetic field orders much of the plasma data. The L shell parameter is used to define the location of a magnetic field line, where each field line is labeled with an L shell value which is the radial distance in planetary radii where the magnetic field line crosses the magnetic equator (see, e.g., chapter 6 of Rossi and Olbert 1970). Lack of azimuthal symmetry in the global magnetic field introduces subtleties in the definition of L which are not important for this review (Schulz and Lanzerotti 1974).

The concepts of supersonic and subsonic plasma flow are of particular importance for understanding the plasma results from Neptune. Plasma is said to be supersonic if the motion of the guiding centers, or the bulk motion, is larger than the thermal speed, or gyromotion. If the plasma is supersonic, it can be observed only by the plasma detectors which are pointed into the plasma flow. This is the case in the solar wind. If the plasma is subsonic then the gyromotion of the particles is faster than the bulk motion of the plasma and particles can enter a detector for all orientations of the instrument. A distinction which is usually made only through the context of the discussion is whether the plasma is supersonic (subsonic) in the nonrotating frame of Neptune or the rest frame of Voyager. The detectability of the plasma is, of course, tied to the plasma parameters as seen in the spacecraft rest frame.

An ion can be added to the magnetosphere either directly, via escape of the ion from a moon's or planet's ionosphere or by direct injection from the solar wind, or indirectly via the injection of neutrals into the magnetosphere (from the planet's or satellite's atmospheres) which are then ionized. Neutrals can be ionized via collisions with electrons, solar ultraviolet photons, or other ions. Ions added directly to the magnetosphere (via escape from a planet's or satellite's ionosphere, for example) keep their original temperatures. Charged particles created from neutrals are quickly accelerated from their original velocity (the Keplerian velocity if they are orbiting the planet) to the corotation velocity. As a consequence of this acceleration these ions gain an initial thermal speed equal to the difference between their initial velocity and the

corotation velocity.

Plasma moves through a planetary magnetosphere by the processes of diffusion and/or convection. Diffusion results from random motions of magnetic flux tubes. Convection can be thought of as an organized motion of magnetic flux tubes, generally inward in some portions of the magnetosphere with compensating outward flow elsewhere. The magnetic field strength in a dipole varies as the distance from the planet cubed. Thus flux tubes which move inward are compressed; those which move outward expand. The volume of a flux tube varies as L^4. Because the plasma is frozen to the field, the density of the plasma increases as the flux tube contracts with an L^{-4} dependence. The plasma is heated as it is compressed; the temperature of isotropic plasma varies as $L^{-8/3}$. This energization process is called adiabatic heating.

B. Pre-Encounter Expectations

With Jupiter, Saturn, and Uranus as a base to draw upon, many predictions were made which applied theories of planetary magnetospheres to the as yet unknown magnetosphere of Neptune (Dessler 1987). Given the experience of the Voyager encounter with Uranus in January of 1986, several early published speculations concerned the remote detection of Neptune's magnetic field via the detection of radio emissions. Both Desch (1988) and Million and Goertz (1988) used the "radiometric Bode's law" and guesses as to Neptune's magnetic moment (~0.5 to 1.0 G at the equatorial "surface") to predict that the total radiated radio power would be $\sim 1.6 \times 10^7$ W and that remote detection of these radio emissions would occur 45 to 90 days prior to closest approach to the planet [29,240 km from the center of Neptune at 0356 UTC, 25 August 1989, equivalently, at 0356 on Day of Year 237 (Stone and Miner 1989)]. Based upon the excess radio emission observed from Neptune at 20 cm, de Pater and Goertz (1989; also Romani et al. 1989) derived a surface equatorial field strength of at least 1 G, assuming the radio excess was due to the synchrotron emission by electrons in a Neptunian radiation belt (this assumption turned out to be false). Unlike Uranus, Neptune showed no evidence of ultraviolet emission which could be associated with auroral activity. Using IUE (the International Ultraviolet Explorer experiment), Clarke (1988) found no evidence of H Lyman-α emission down to a 1σ limit of 180 Rayleighs (some implications of this were discussed by McConnell et al. [1989] prior to the encounter). Although this non-observation could not rule out an active magnetosphere per se, it did rule out processes similar to those associated with the electroglow and/or aurorae observed at Uranus (see, e.g., Yelle et al. 1987). This low intensity was confirmed by Voyager observations (Broadfoot et al. 1989).

The lack of ultraviolet and radio observations led Dessler and Sandel (1989) to speculate that the magnetosphere of Neptune could be quiet if the mass loading by internal plasma sources were ≤ 1 kg s^{-1}. They noted that Neptune's internal heat source combined with the scalings noted above should lead to a large dipole moment of at least 1 G R_N^3 that was spin-aligned with little offset.

Radio emissions from Neptune were finally identified eight days before closest approach in data from the planetary radio astronomy experiment (Warwick et al. 1989; Stone and Miner 1989). A re-examination of the data revealed that radio bursts were present beginning 30 days prior to closest approach. This was the first indication that Neptune had a well-developed magnetosphere.

Science sequencing for the Neptune encounter was based on the assumption that a spin-aligned dipole magnetic field was the most likely configuration. This magnetic orientation implied that the spacecraft could pass through the Neptunian auroral zone near closest approach. Scaling arguments (Cheng 1989) suggested that auroral electrons with energies of tens of keV could be streaming from the magnetosphere into the ionosphere. Based on these expectations the spacecraft was rolled to enable the PLS experiment to detect precipitating plasma (plasma moving downward along the magnetic field) near closest approach; the trade off was a possible loss of information about cold, corotating plasma in this region.

The study of Triton was one of the primary encounter goals; one reason was its possible role as a source of magnetospheric plasma. Groundbased observations detected methane (Cruikshank and Silvaggio 1979) and nitrogen (Cruikshank et al. 1984) on Triton. Delitsky et al. (1989) modeled the escape, ionization, and loss of nitrogen and methane from Triton and predicted the formation of a torus of mainly H^+ and N^+ with a density of 1 to 8 cm^{-3}. These predictions, although larger than the observed densities, provided a good basis for understanding the plasma observations obtained during the encounter.

C. Instrument Description and Analysis Methods

Some knowledge of the characteristics of the PLS instrument is necessary in order to understand the results and limitations of the plasma data; a full description of the instrument is given by Bridge et al. (1977). The instrument consists of four modulated-grid Faraday cups which measure current as a function of energy/charge. Three of these cups (A, B, and C) form three faces of a tetrahedron, each facing 20° from an axis which points toward Earth. The D cup looks at right angles to this axis and was oriented at the encounter to look approximately into the direction of corotation inbound and outbound from Neptune and upwards (away from Neptune) near closest approach. The instrument covers the energy-per-charge range of 10 to 5950 V. A sample spectrum from Neptune's magnetosphere is shown in Fig. 1. It was obtained with the D cup at about 10 R_N from Neptune and shows the current detected as a function of energy-per-charge. Although the instrument cannot directly determine the ion mass, this spectrum shows how, in practice, ion species can be identified. If all ion species move with the same bulk velocity (as expected from the "frozen-in" law) the energy of each ion is proportional to its mass. The PLS instrument measures energy-per-charge, so the peaks of the

measured currents of ions with different masses are separated by the ratio of their mass/charge. Assuming the plasma in Fig. 1 is corotating, the energies of the peaks correspond to ions with mass/charge ratios of approximately 1 and 14. As Triton is thought to be a major source of H and N, these current peaks are presumed to be H^+ and N^+ (although other ions with similar mass, e.g., C^+ or O^+, are possible). The width of the ion peaks is proportional to the ion temperature, so that if the plasma is hot the ion peaks merge and determining the composition is much more problematic. This is the situation near closest approach to Neptune, as will be discussed in Sec. IV.A.

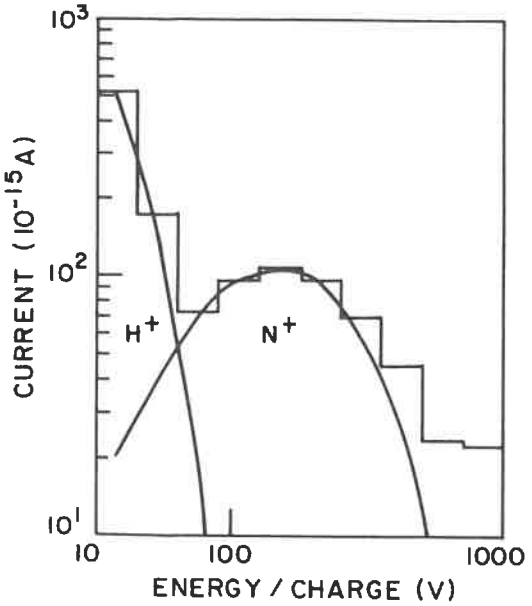

Figure 1. An L mode spectrum from the first plasma sheet crossing taken at 0018 UT on 25 August. Measured ion current from the D sensor is plotted versus energy. The curves show the best fit to the data obtained assuming two ion species, H^+ and N^+, which have convected isotropic Maxwellian velocity distributions and corotate with the planet.

The ions are measured using two modes, the low energy/charge resolution L mode ($\Delta V/V \approx 29\%$) and the high energy/charge resolution M mode ($\Delta V/V \approx 3.6\%$). In each mode, ion spectra are obtained simultaneously in each of the four cups. A set of high-resolution M mode spectra is obtained once every 12 min and 25 sets of low-resolution L mode spectra are obtained during each 12 min period. Twelve sets of the L mode spectra (denoted L-short) are obtained using a short integration time (0.21 s per channel) and 13 sets (denoted L-long) are obtained with a longer integration time (0.93 s per channel). This scheme is the same as that used during the Voyager 2 encounter with Uranus [see, e.g., Table 1 of Sittler et al. (1987)] and was selected to increase the dynamic range of the instrument for observation of an unknown plasma environment.

The goal of the data analysis is to determine the bulk plasma properties, i.e., the density, velocity and temperature of each plasma component. This can be accomplished in two ways. The first is to take the moments of the distribution function; the second is to fit the observed profile with a model distribution (Vasyliunas 1971). The parameters shown in this chapter are derived using the second method under the assumption that the plasma distribution is well represented by a summation of convected isotropic Maxwellians. A nonlinear least squares fitting routine is used to find the plasma density, temperature, and velocity which, when combined with the instrument response, best fit the data. The data quality limits the accuracy to which these values can be determined. Signal must be observed in at least three cups for the full velocity vector to be determined. This is the case in the solar wind and magnetosheath. In the magnetosphere, data quality allows us to determine the azimuthal component of velocity only outside $L \approx 7$; inside this we cannot determine the velocity and so assume that the velocity equals the rigid corotation speed in order to analyze the data. A sample fit is superimposed on the data in Fig. 1 and shows good agreement between the simulated and observed currents.

Electrons are only measured in the D cup; because the electron thermal speed is much greater than the bulk velocity of the plasma, the look direction of the cup does not affect the measurements as long as the distribution function is isotropic. Two energy scan modes, the low energy $E1$ mode (10–140 eV) and the high energy $E2$ mode (140–5950 eV), are employed. Both energy modes consist of 16 contiguous energy channels which are used to obtain differential distributions of the electron flux into the D cup. The sampling time for each channel is 0.21 s for the short integration ($E1$ short and $E2$ short) modes and 0.93 s for the long integration ($E1$ long and $E2$ long) modes. We will present only results from the long-integration-time modes. The effective time resolution is 96 s, but this time resolution is further affected by interference associated with spacecraft operation, which renders about one sixth of the electron spectra unusable. Thus the actual time resolution of the electron data we obtain is about 2 min. The electron density and temperature are determined by fitting isotropic Maxwellian distributions to the data. One to three Maxwellians are used, as needed, to characterize the electron population in each spectrum. A sample electron spectrum from the magnetosphere at 0659 UT on day 237 is shown in Fig. 2, along with the curve showing the Maxwellian distributions which best fit this data. In this case three Maxwellians are required to provide a full description of the measured electron distribution function.

II. OVERVIEW OF THE ENCOUNTER

Plates 6 and 7 show spectrograms of the ion and electron currents obtained

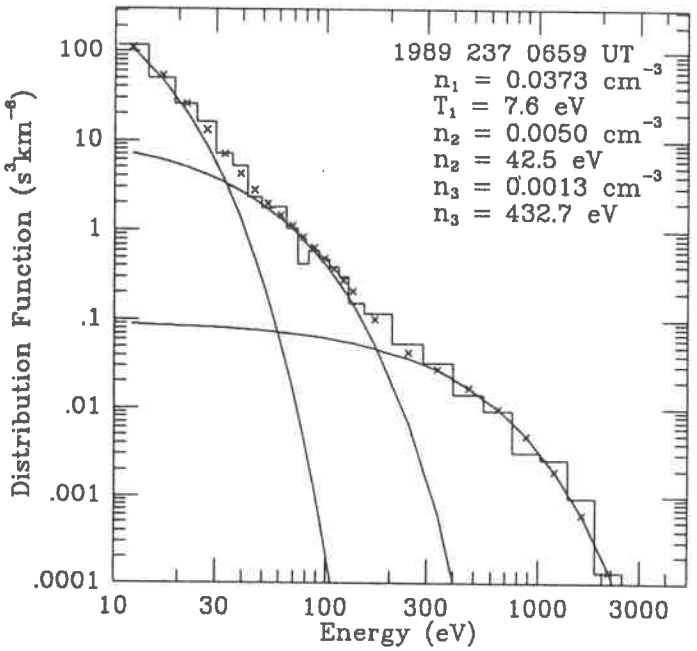

Figure 2. An example of an electron spectrum in the magnetosphere and the the best fit to this data. Three Maxwellian distributions were required to fit the currents in this spectrum; they are shown by the solid curves. The x's show the summed current from the fit.

during the encounter with Neptune. Each of the four panels shows time increasing across the panel to the right and energy increasing upwards, with the intensity of the current at each location in energy-time space indicated by the color, as described by the color bar. As a rough approximation, the height of the plasma signal in energy is proportional to the plasma velocity, the width of the signal is proportional to the temperature, and the intensity of the current is proportional to the density. The panels, from top to bottom, show the high-energy (140–2480 eV) electrons ($E2$ mode), low-energy (10–140 eV) electrons ($E1$ mode), ions in the side-looking detector (D cup, L mode, 10–1850 eV), and ions in one of the earthward looking detectors (C cup, L mode, 10–1850 eV). The higher energies are not shown because the true signals have a low amplitude and are typically contaminated by noise. Both electron and ion spectra are from the long integration modes. In Plate 6 each time step (1 pixel wide in the original computer-generated image) shows the average of 4 spectra; in Plate 7, in which the scale is compressed, each time step shows the average of 12 spectra. The apparent signal in the highest few channels of the C cup is usually noise. The intense fluxes of ~850 eV ions in the C cup before the inbound bow shock at 1438 UT (coordinated universal time at Voyager) on day 236 and after the outbound bow shock at 2036 on day 238 are the solar wind protons. Inbound, the solar wind velocity is relatively constant; outbound, the velocity is more variable. Across the bow shock the solar wind plasma changes from a supersonic stream covering only a few energy channels to a hot population visible in the spectrogram as a very broad distribution in energy in the C cup. This hot region after the bow shock crossing is called the magnetosheath. The electrons, which are too cold to be detected in the solar wind, appear in the low-energy electron spectra after Voyager enters the magnetosheath.

At the other planets encountered by Voyager the transit through the magnetosheath ended abruptly when the magnetopause was crossed. This transition was marked by a dropout in the plasma fluxes. At Neptune, however, the density and temperature of both ions and electrons began a gradual decrease at 1800 UT on day 236 of 1989, with a complete dropout of the plasma signal not occurring until 1920 UT. This signature, combined with the knowledge that Voyager passed through this region when the magnetic pole of Neptune was pointed towards the Sun, indicates that Voyager encountered the cusp (Belcher et al. 1989; Ness et al. 1989; Szabo et al. 1991). The cusp is the region of open magnetic field lines associated with the magnetic pole and is described further in Sec. III.C.

Inside the magnetosphere proper, ion and electron fluxes were below the instrument threshold from the magnetopause to 2200 UT on day 236 (15 R_N from the planet inbound). Starting at this time, the PLS experiment detected first energetic electrons, then lower-energy electrons, and finally ions (Belcher et al. 1989; Richardson et al. 1991). The largest ion fluxes in this region appear in the D cup, which pointed into the corotation direction. Electrons with energies above 40 eV disappear just before 0030 UT on day 237 (10 R_N); lower-energy electrons remain until 0200 UT (5 R_N), and ions until 0300 UT (3 R_N). After closest approach, hot ions and electrons reappear simultaneously at 0412 UT on day 237. Fifteen minutes later all but the lowest-energy ions disappear. Two ion components and electrons are again detected at 0435 UT; they are hot, but less so than earlier. The ions cool as the spacecraft moves outward; the abrupt increase in ion flux at 0550 UT (5.5 R_N) in the D cup is an artifact caused by a roll of the spacecraft which oriented the D cup so that it looked into the corotating flow (Richardson and McNutt 1990). Electron fluxes become more intense near 0730 UT (10 R_N). Mirroring the inbound sequence, first the ion flux, then the low-energy electron flux, and finally the high-energy electron flux decrease to below the instrument threshold. No signature associated with the closest approach to Neptune's large moon Triton at 0910 UT on day 237 was detected in the PLS data. A feature in the electron data is centered at 2100 UT on day 237. This enhancement of 10 to 20 eV electrons may be a crossing of the plasma mantle; it is observed one planetary rotation before the first mantle encounter reported by Zhang et al. (1990). (The plasma mantle, which will be discussed in detail in Sec. V, is a high-latitude region between the magnetosheath and magnetosphere which has a mixture of the characteristics of each region.) At 0800 UT on day 238,

Voyager crossed the magnetopause into the downstream magnetosheath. The plasma here is supersonic, although hotter than in the solar wind. After the bow shock crossing at 2036 UT the spacecraft is in the solar wind. Several more possible bow shock crossings occurred through 0900 UT on day 240 (Belcher et al. 1989).

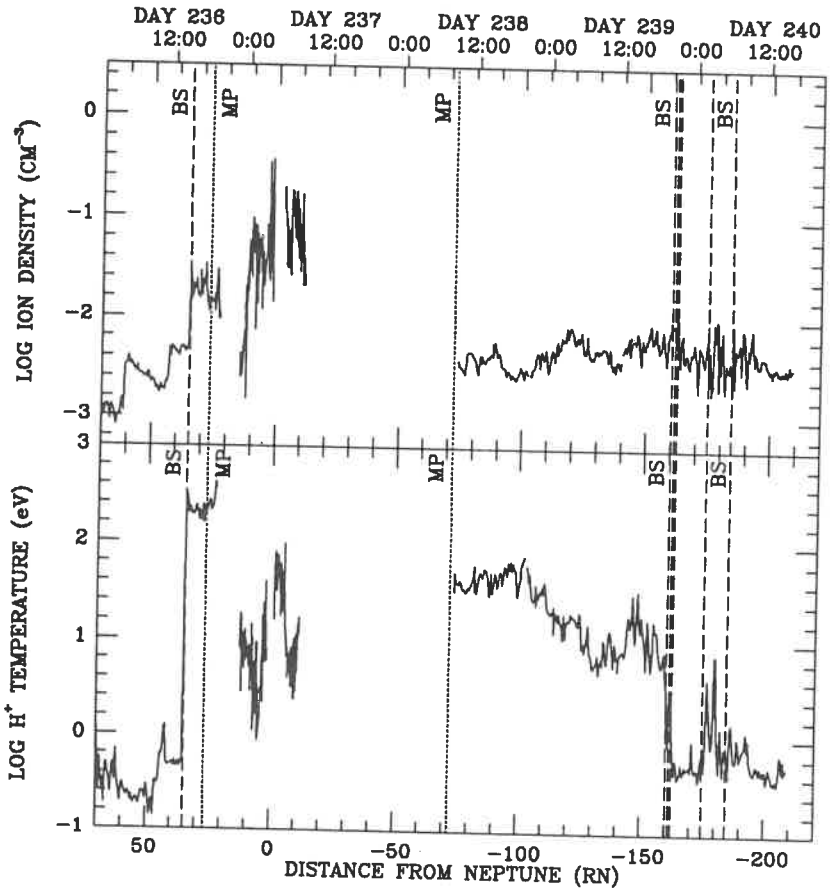

Figure 3. Quantitative overview of the encounter showing the total ion density and the proton temperature. The dashed and dotted lines indicate the bow shock (BS) and magnetopause (MP) positions, respectively.

Figure 3 provides a more quantitative overview of the plasma data, showing the plasma density and proton temperature throughout the encounter period. The dashed and dotted lines indicate bow shock and magnetopause positions, respectively, as determined by Belcher et al. (1989). The densities shown are the total ion density, if available, and the total electron density otherwise. In the magnetosphere the spectra were individually fit with Maxwellians. Inside 140 R_N outbound, the M mode fluxes were too low to calculate plasma parameters, so we show values derived from L mode spectra. Because even L mode fluxes are very low in this region, it was necessary to average 12 minutes of data (13 spectra) to improve the signal to noise ratio sufficiently to analyze these spectra. Comparison of L and M mode parameters when both are available shows good agreement, indicating that the lower energy resolution of the L mode does not diminish the accuracy of the results.

The measured densities and temperatures span several orders of magnitude. The densities vary from 10^{-3} cm^{-3} in the solar wind to a maximum of 2 cm^{-3} in the magnetosphere. At the inbound shock the density increases by a factor of 4 (this is typical for a high Mach number shock). Outbound, the density change across the shock is insignificant compared to the density variations in the magnetosheath and solar wind. Inbound, the H^+ temperature increases from 0.5 eV in the solar wind to a few hundred eV in the magnetosheath and cusp. Outbound, temperatures are near 5 eV in the magnetosheath and then decrease to 0.8 eV in the solar wind. The bow shock is not clearly defined in the downstream region; the increase in temperature between 175 and 184 R_N probably corresponds to another entry into the magnetosheath (Belcher et al. 1989; Ness et al. 1989).

III. DAYSIDE INTERACTION OF THE MAGNETOSPHERE WITH THE SOLAR WIND

A. The Inbound Bow Shock

Voyager 2 approached Neptune close to the planet-Sun line and crossed the planetary bow shock on 24 August 1989 at 1438 UT when it was 34.8 R_N from Neptune (Belcher et al. 1989). The bow shock occurs where the solar wind flow is first affected by the planetary magnetosphere; at the shock the plasma slows down and is heated as the plasma flow changes from supersonic to subsonic. This transition enables the plasma to change direction and flow around the magnetosphere.

The upstream conditions of the solar wind were steady for a number of hours before the bow shock crossing ($V \approx 420$ km s^{-1}, $n \approx 0.005$ cm^{-3}, $T_p \approx 0.5$ eV where V is the solar wind speed, n the number density of protons and T_p the proton temperature). The interplanetary magnetic field was also stable during this period, with a magnitude of 0.14 nT pointed approximately perpendicular to the planet-Sun line in the solar equatorial plane.

The electron temperature is not known because electrons are too cold to be observed in the solar wind this far from the Sun. (the energy of the bulk of the electrons is well below the 10 eV threshold of the PLS instrument). Using observations made closer to the Sun, Sittler and Scudder (1980) derive an empirical polytrope law (an equation relating the density and temperature) based on electron parameters obtained between 0.45 and 4.76 AU. For the solar wind density observed upstream of the Neptunian bow shock, this polytrope law predicts a thermal electron temperature of 2.1 eV. This value for the electron temperature gives upstream values for β, the ratio of plasma thermal

energy (nkT) to magnetic energy ($B^2/8\pi$), of 0.19 for electrons, 0.04 for protons, and 0.23 for the plasma as a whole.

Table I shows the values of plasma parameters in the upstream and downstream regions, plus various Mach numbers and scale lengths discussed later.

Figure 4 shows profiles of the magnetic field magnitude, the plasma flow velocity, the ion and electron densities, and the ion and electron temperatures measured through the shock. One standard deviation error bars are shown in the magnetosheath (after 1438 UT on day 236); elsewhere errors are smaller than the plot symbols. The location of the shock is quite apparent from the plot. The nonlinear least squares solution of the "Rankine-Hugoniot Problem," derived by Vinas and Scudder (1986) and improved by Szabo (1994), is used to determine the geometrical properties of the shock (i.e., the direction of the shock normal, the angle between the shock normal and the local interplanetary magnetic field direction, and the bulk speed of the shock), the conservation constants, and the self-consistent asymptotic magnetofluid variables. The advantage of this technique is that it establishes the uniqueness of the solution. The improved fitting technique incorporates the normal momentum flux and energy flux conservation equations; therefore it is possible to fit the total plasma temperature as well as the other plasma and magnetic field parameters. The best fit solution gives a shock normal direction of ($R = -0.999\pm0.001$, $T = -0.001\pm0.009$, $N = 0.030\pm0.014$) in a Neptune-centered, non-inertial, heliographic system (Szabo and Lepping 1994). The RTN system is defined such that the R axis points radially outward along the Sun-Neptune line, the T axis lies in the solar equatorial plane pointing in the direction of Neptune's motion, and the N axis completes a right-handed system, pointing northward. Thus the shock normal points almost directly along the Sun-planet line. The angle between the interplanetary magnetic field and the shock normal is $58.2°\pm2.3°$, so this is a quasi-perpendicular shock. The bulk speed of the shock along the shock normal is 15 ± 12.0 km s^{-1} outwards (towards the Sun). The best fits for the asymptotic magnetofluid variables are shown by solid lines in Fig. 4; the dotted lines represent 1σ standard deviations. The agreement between the fit results and the measured values is very good (note that only the first hour of data in the magnetosheath is used for the fits), demonstrating that the MHD Rankine-Hugoniot description of a quasi-perpendicular shock is an excellent approximation of Neptune's bow shock upstream of the planet.

The Szabo nonlinear least squares technique cannot determine the individual proton and electron temperatures, only the total plasma temperature (showed by solid lines on Fig. 4). The values of the total plasma temperature obtained with the model compare well with the measured value of 2.6 eV upstream (if the electron temperature is estimated as described above) and 235.7 eV downstream.

Once the bulk speed of the shock and the average values of the magnetofluid variables are known, the various Mach numbers associated with the

TABLE I

Observed Plasma Parameters Across the Neptunian Bow Shock

Plasma Parameters	Definition	Up	Down
n, cm^{-3}		0.0046±0.0003	0.019±0.003
T_i, eV		0.49±0.04	208±28
T_e, eV		< 2.1*	28±4
V, km s^{-1}		419.3±0.2	97±13
$U \equiv V_\perp - V_{shock}$, km s^{-1}	$V_{shock} = -15.0 \pm 12.0$ km s^{-1}	433.6±12.1	107.6±17.7
$B_\parallel$, nT		0.14	0.52
$\beta_T = \beta_e + \beta_i$	$\beta_T \equiv 8\pi nk(T_e + T_i)/B^2$	<0.23	6.2±1.4
$M_S \equiv U/C_S$	$C_S^2 \equiv \gamma kT_e/m_p$	>30.6	2.09±0.37
$M_A \equiv U/V_A$	$V_A^2 \equiv B^2/4\pi nm_p$	9.4±1.2	1.26±0.25
$M_{MS} \equiv U/C_{fms}$	$C_{fms}^2 \equiv C_S^2 + V_A^2$	>8.95	0.72±0.13
r_{ge}, km		<33.9	33.1±3.5
r_{gi}, km		706±92	3870±395
c/ω_{pi}, km		3360±110	166±115
$r'_{gi} = U_{Upstream}/\Omega_{ci}$, km		31,400±4000	8400±700

* Based on extrapolated polytrope model.

value. The details of this oscillation are hard to characterize, but the wavelength of the first oscillation appears to be around 22,900±3300 km, about one upstream ion gyroradius r'_{gi} and 3 times the downstream value of r'_{gi}, consistent with results at Uranus and at Earth (Bagenal et al 1987; Scudder et al. 1986*a*).

B. The Inbound Magnetosheath

After the solar wind plasma is heated and slowed to subsonic speeds by the bow shock, it traverses the turbulent regions of the magnetosheath as it flows around the magnetopause. The plasma and magnetic field are still those of the solar wind, but their nature is significantly altered by their passage through the shock. The plasma parameters in the inbound magnetosheath derived from the Voyager observations are summarized in Fig. 5. We expect that, to first order, the flow around Neptune's magnetosphere should be well described by the gasdynamic convected magnetic field approximation to the magnetohydrodynamic model for supersonic solar wind flow past a planetary magnetosphere. The gasdynamic model has been very successful at modeling magnetosheath plasma at other planets both with and without magnetospheres (Spreiter et al. 1966; Spreiter and Stahara 1985; Slavin et al. 1985; Russell 1985; Stahara et al. 1989). Computational techniques developed for use at Earth (Spreiter and Stahara 1980*a*, *b*; Stahara et al. 1980) are used by Stahara to provide the solution for the detailed flow and magnetic field properties throughout the Neptunian magnetosheath (Richardson et al. 1994). The model values along the spacecraft trajectory are shown by the solid lines in Fig. 5. The inputs provided to the model are the measured Mach number (listed in Table I), the magnetopause location, and a value of 2 for γ, the ratio of the specific heats. The model was configured to calculate magnetosheath parameters for a magnetopause which is axisymmetric about a line which is parallel to the incident, aberrated (corrected for the orbital motion of Neptune) solar wind direction and which passes through the center of Neptune. The location of the magnetopause is taken from the Voyager measurements. The gasdynamic model slightly overestimates the width of the inbound magnetosheath; this could be corrected for by allowing values of γ slightly below 2 (but still larger than 5/3), consistent with findings at other planets (Slavin et al. 1983) and with the results of the Szabo MHD bow shock fitting technique which gives γ=1.9 upstream from the shock (Szabo and Lepping 1995), or by allowing a nonaxisymmetric magnetopause shape, as is observed in the case of Jupiter and Saturn (Stahara et al. 1989). However, the plasma bulk velocity, density and magnetic field components are modeled quite well to first order. The model overestimates the plasma temperatures, a problem also encountered in the case of the other gas giants and which appears to be a limitation of the gas-dynamic model. Differences between the model and the actual measurements near the inbound bow shock are due to the microstructure of the shock described in the previous section. Close to the inbound magnetopause, the deviations from the model predictions and the unexpected systematic cooling of the plasma temperature throughout the magnetosheath may be explained by a slow mode expansion fan characteristic of open magnetospheres. (A slow mode expansion fan is a region which is expanding in size at the slow mode speed. In this case the inside of the fan is a region where magnetosheath and magnetospheric plasma mix. The size of this region, which is the plasma mantle, increases from a point in the subsolar region to a layer which nearly fills the magnetotail far downstream of the planet.) This observation is consistent with the identification of the Neptunian magnetopause as a rotational or rotational-like discontinuity (Szabo et al. 1991; Lepping et al. 1992).

C. The Inbound Magnetopause and Cusp

The strongly tilted and offset magnetic dipole of Neptune, as reported by Ness et al. (1989), creates the unique situation of a subsolar magnetic cusp region which recurs once per Neptunian day (16.11 hr). The fortunate timing of the Voyager 2 encounter with the boundary of the magnetosphere, the magnetopause, offers the opportunity to study the plasma environment of this region. A rapid 45° rotation of the magnetic field marks the magnetopause location at 1800 UT of day 236. The estimated thickness of the magnetopause is 5100 km (2 proton gyroradii), consistent with the average magnetopause thickness of the five other magnetized planets. The total magnetofluid pressure is in balance across the magnetopause; an observed moderate imbalance in the normal momentum flux can be accounted for by a reasonable thermal anisotropy change across the boundary. Magnetic field variance and MHD discontinuity studies reveal that the Neptunian magnetopause is a rotational or rotational-like discontinuity (Szabo et al. 1991; Lepping et al. 1992) which allows some plasma to flow from the magnetosheath into the magnetosphere, forming the dynamic mantle layer. This layer is characteristic of open magnetospheres and has been extensively studied in the case of Earth's cusp (Paschmann et al. 1976; Siscoe 1988). The open magnetosphere model hypothesis is further supported by a decrease in the proton and electron densities prior to the magnetopause crossing (see Fig. 5), which may indicate that magnetosheath plasma leaks into the magnetosphere. The plasma densities continue to decrease through the cusp region and drop below the instrument threshold shortly after the crossing of the inner boundary of the cusp at 1930 UT. The magnetic field magnitude concurrently increased, characteristic of a slow mode expansion fan, until it reached the magnetospheric dipole values. The temperature of the protons increased in the cusp, while the anti-sunward component of the plasma bulk flow dropped to zero. The estimated width of the cusp based on the geometry of the crossing is 26.5 R_N (Lepping et al. 1992).

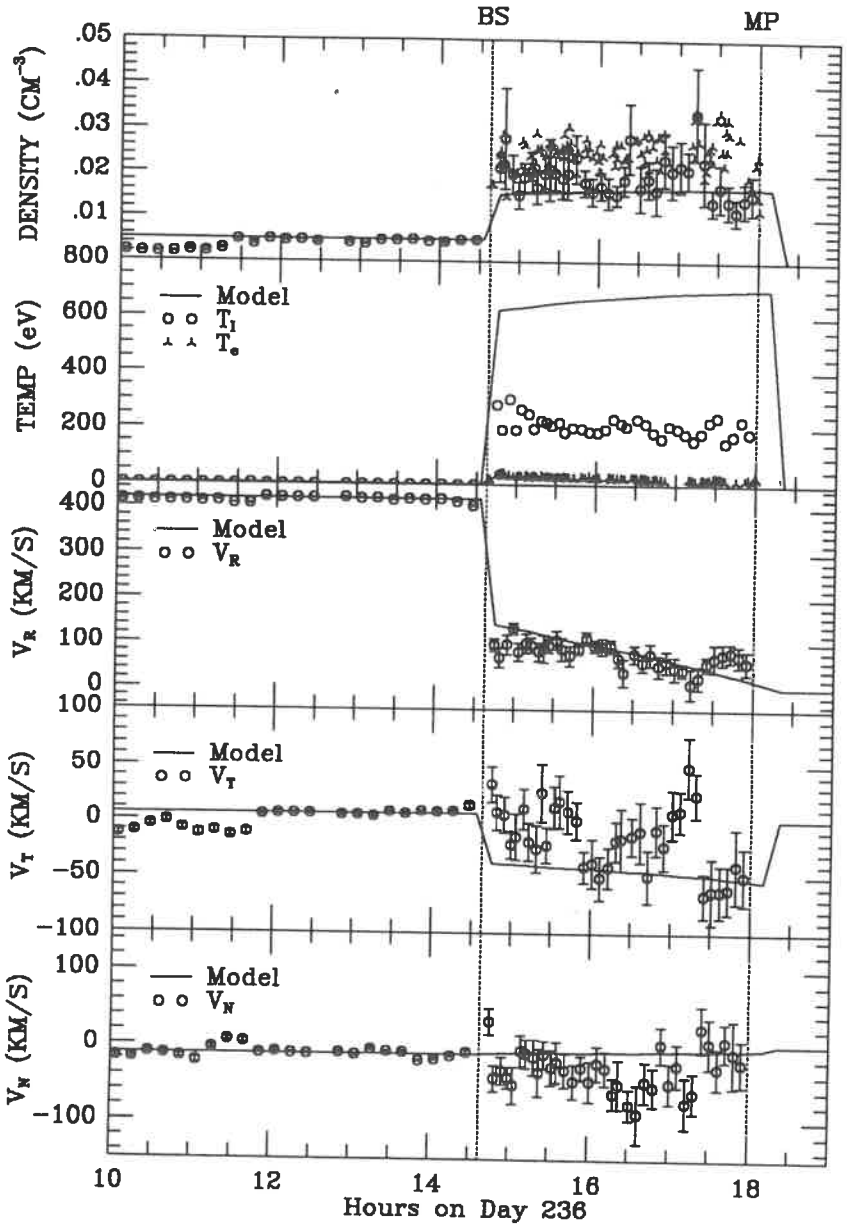

Figure 5. Voyager 2 measurements of the plasma bulk velocity, electron and ion number densities, and temperatures in the Neptunian magnetosheath and cusp. The predictions of gas-dynamic theory are shown with solid lines.

IV. THE MAGNETOSPHERE: DATA

A. PLS Data From The Magnetosphere

Although plasma parameters in general are best organized by the magnetic field L shell, the values of L depend on the magnetic field model. Therefore, magnetospheric parameters are first presented as plots versus radial distance from Neptune.

1. Data Analysis. The ion spectra outside 6 R_N often contain two distinct current peaks (as in Fig. 1). We assume that the ion species are H^+ and N^+ and that the ion distribution functions are convected isotropic Maxwellians; this allows us to determine the densities and temperatures of each species and the azimuthal velocity of the plasma as a whole. Insufficient information is available to determine the nonazimuthal velocity components or the anisotropies of the ion distribution functions. The electron parameters are found by fitting the electron spectra with a cold Maxwellian component plus one or two hot Maxwellian components.

A serious difficulty that affects both the ion and electron analysis is that the spacecraft has a negative potential which is on the order of 10 V. This potential depresses the thermal electron current entering the instrument, causing the density of these electrons to be underestimated, and accelerates ions into the detector, causing the ion velocity to be overestimated. This effect is not taken into account in the calculation of the ion parameters which follow but is discussed in more detail in Sec. IV.A.4. The electron densities shown are compensated for charging through use of the requirement of charge neutrality to determine the total electron density (total electron density equals the total ion density).

2. Magnetospheric Plasma Parameters. Figure 6 shows the H^+, N^+, and electron densities with 1σ error bars [estimated from the variance in the fits (see Bevington 1969)] plotted versus radial distance from Neptune. Figure 7 shows the temperatures of these three components of the plasma. Negative values of R indicate Voyager was approaching Neptune and positive values that Voyager was moving away from Neptune. The dotted lines show crossings of the magnetic equator as determined by the magnetometer (MAG) experiment.

Inbound, proton fluxes are first detected at 12.5 R_N. The density increases to a maximum of 0.1 cm^{-3} at 9 R_N, and then decreases slowly inward until the flux level falls below the detection level of the PLS instrument at 2.5 R_N. Ion fluxes are below the PLS threshold between 4.2 and 5.4 R_N. Outbound, the density increases rapidly from 0.01 cm^{-3} near closest approach to almost 0.4 cm^{-3} in a narrow peak at 0420 UT, just prior to the crossing of the magnetic equator. After this peak, the density falls by a factor of 20 to 0.03 cm^{-3} at 2 R_N, increases to 0.2 cm^{-3} at 3 R_N, then decreases to 0.04 cm^{-3} at 6 R_N where there is a sharp rise to 0.15 cm^{-3}. After this the densities gradually decrease until the ion flux falls below the instrument threshold at 11.3 R_N.

The N^+ density profile is qualitatively very similar to the H^+ profile,

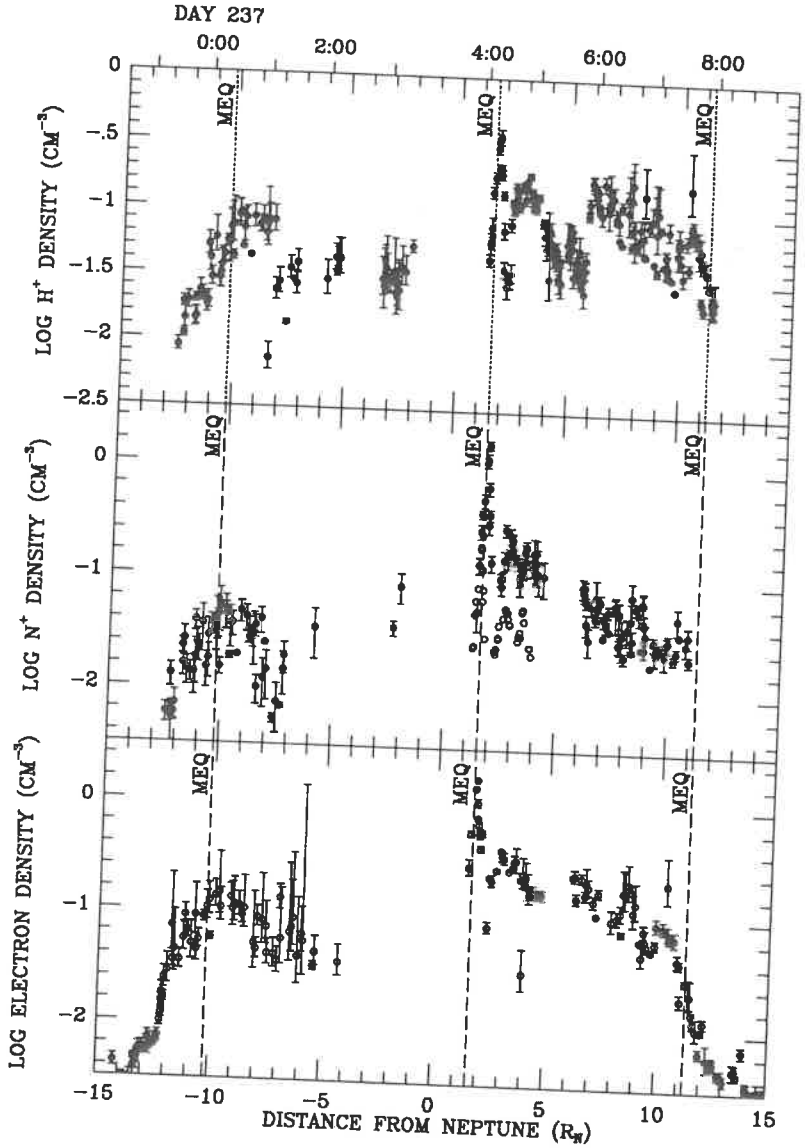

Figure 6. The densities of H^+, N^+, and electrons in the magnetosphere as a function of radial distance from Neptune with 1σ error bars. The open circles in the middle panel indicate the density if the hot ions near Neptune were H^+ instead of N^+.

with a peak at $9\,R_N$ inbound and relatively high densities just after closest approach which decrease as Voyager moves away from Neptune. Although the H^+ density is almost twice the N^+ density outside $5\,R_N$, near the planet the N^+ density is larger, with a peak density of 1.6 cm^{-3} near closest approach.

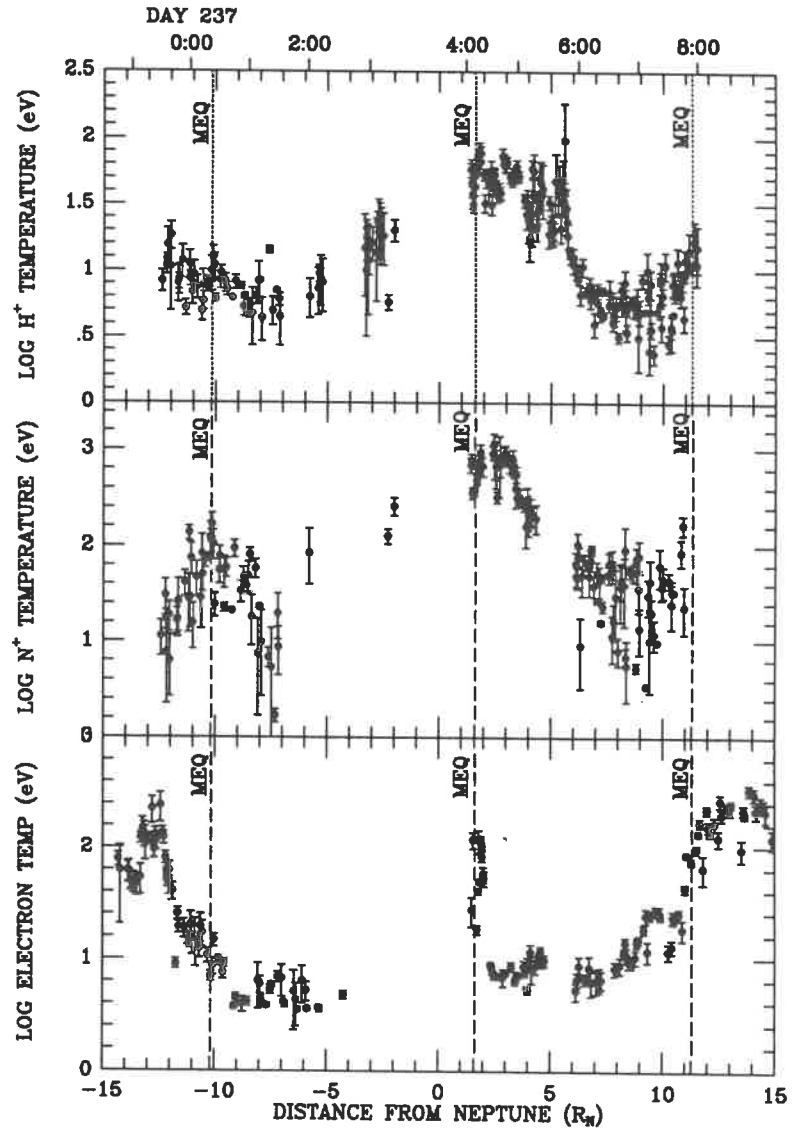

Figure 7. The temperatures of H^+, N^+, and electrons in the magnetosphere as a function of radial distance from Neptune with 1σ error bars.

The open circles in the middle panel of Fig. 6 show the densities of the hot component if these ions were hot protons; error bars are omitted to avoid cluttering the plot. Although, as discussed below, we believe these ions are N^+, the spectra are so hot that other species, including H^+, cannot be ruled out and give equally good fits to the data. The H^+ densities would be, on

average, a factor of $\sqrt{14}$ below the N^+ densities. The maximum density is 0.27 cm^{-3}, substantially less than the 1.6 cm^{-3} for N^+. The temperature of the ions would be approximately the same for either H^+ or N^+.

Electrons are first detected in the inner magnetosphere at 14.4 R_N where their density is 2.5×10^{-3} cm^{-3}. This is well before the first detection of ions at 12.3 R_N. Starting at 12.2 R_N, the electron spectra contain a cold component. As the temperature of this cold component is comparable to the spacecraft potential, densities derived from these electron spectra are seriously affected by the spacecraft charge. Thus ion data provide the only reliable density estimates in this region; the total electron density shown in Fig. 6 is obtained by summing the ion components when ions are observed; otherwise it is from the electron measurements but not corrected for the spacecraft potential. Between 12.2 and 9.6 R_N the electron density increases from 0.01 cm^{-3} to 0.1 cm^{-3} and the electron temperature decreases from 25 eV to 7 eV. At 9.2 R_N the cold electron component disappears, and only a minor hot electron component is present in the spectra. The electron density derived from the fits has a clear discontinuity at this point, but the ion density does not show any change. The likely explanation is that the thermal electrons cool below the instrument's energy threshold. For electrons with a density of 10^{-2} cm^{-3} this implies the temperature was less than 3 eV. The total electron temperature shown in Fig. 7 is an upper limit obtained by setting the temperature of the cold component to 3 eV and computing the weighted average of these electrons and the hot electrons. The density of cold electrons is the total electron density (derived from the ion density) minus the hot electron density. Inside 3.9 R_N, the electron measurements show only background noise until closest approach. Even though ions are observed near 3.1 R_N, the electron spectra in this region cannot be analyzed and the electron temperature is unknown.

The plasma detected by the PLS instrument at 1.8 R_N, near the magnetic equator crossing, is hot and relatively dense. The maximum electron density and temperature are 2 cm^{-3} and 90 eV, respectively. This is followed by a low plasma density region starting at 0427 UT of day 237 (which may be due to ring absorption, see below) where the electron spectra cannot be analyzed. The electrons become cold again at 0435 UT. The electron parameters through the rest of the outbound trajectory are similar to those observed inbound at the same radial distance.

The proton temperature profile is roughly symmetric inbound and outbound. Inbound, the temperature decreases inward from 15 eV at 12.5 R_N to 5 eV at 7 R_N and then increases to 50 eV near closest approach. Outbound, the density decreases from a maximum of 50 eV near closest approach to a minimum of 5 eV at 8 R_N, and then increases to just over 10 eV at 11 R_N. The N^+ temperature increases as Voyager approaches Neptune, then decreases as Voyager moves away from the planet. The thermal speeds of N^+ and H^+ are comparable, with the proton thermal speeds slightly larger (Richardson and McNutt 1990). Because N^+ has a larger mass, the N^+ temperatures are much higher than those of H^+, 100 eV outside 5 R_N and 700 eV near Neptune.

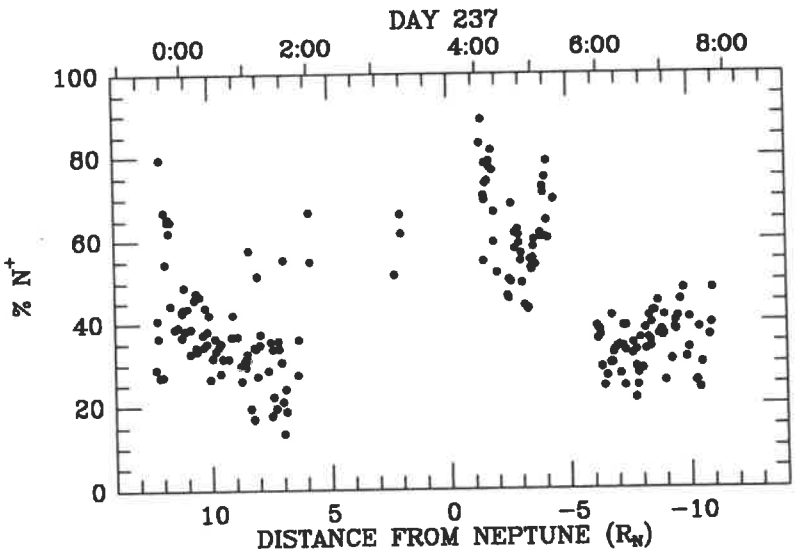

Figure 8. The percentage of ions which are N^+ as a function of radial distance from Neptune.

Figure 8 shows the percentage of ions which we identify as N^+. Outside 5 R_N the plasma averages 40% N^+; inside this about 60% of the ions are N^+ (assuming the hot component in this region is N^+).

Figure 9 shows the azimuthal velocity and formal 1σ error bars derived from fits to spectra which have two distinct current peaks. The solid line shows the corotation velocity V_ϕ; points on this line with no error bars indicate places where fits were performed assuming rigid corotation. Inbound velocities average about 20 km s^{-1} above the corotation value; outbound the values show much more scatter, ranging from 0.5 to 3 times corotation. As indicated above, we believe that this deviation from corotation is an artifact resulting from a negative spacecraft potential which averages about 10 V.

3. Cold and Hot Electrons. Because the electron spectra in the magnetosphere are not well described by a single Maxwellian, the total electron density and temperature do not provide complete information about the electron distribution function. Most of the electron spectra in Neptune's magnetosphere can be simulated using a cold Maxwellian component and several hot Maxwellian components, as shown in Fig. 2. Figure 10 shows the temperature of the cold electrons (T_c), the hot electrons (T_h), and the ratio of the hot electron density (n_h) to the total electron density (n_e). Like the total electron temperature, T_c decreases towards closest approach. The three hot plasma regions which have no thermal electron components have a ratio n_h/n_e=1. When cold electrons are present, hot electrons are a small fraction of the total population; the ratio n_h/n_e is usually a few percent. The hot electron temperature is calculated

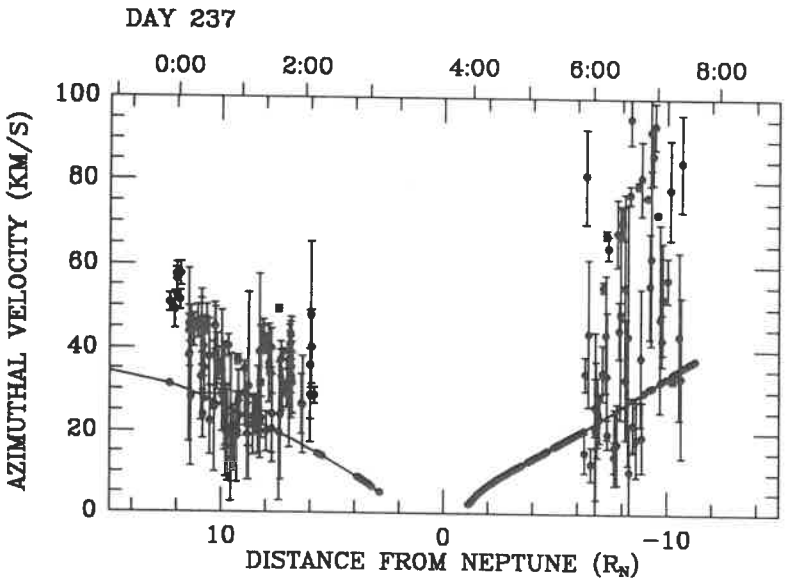

Figure 9. The azimuthal velocity derived from spectra which have distinct light and heavy ion peaks. The solid line shows the corotation velocity. The dots on the corotation line with no error bars show the location of other fits.

using one or two hot Maxwellian distributions to fit the nonthermal portion of the data, then taking a weighted average of the temperatures. For most of this time period T_h is 100 to 200 eV. Although small in density, the hot electrons are important contributors to the ionization of neutral atoms in Triton's torus as the ionization rates of hydrogen and nitrogen peak for electron temperatures near $T_e = 300$ eV.

4. Spacecraft Charging. We mentioned previously that the spacecraft had a small negative charge in the magnetosphere. This causes the total density obtained from fits to the electron spectra to be less than the ion density. The condition of charge neutrality is used to determine the spacecraft potential when a value of the cold electron density (which is less than the actual value because of the potential) can be determined from the spectra. To first approximation, the spacecraft potential (Φ_{SC}) is (Zhang et al. 1991)

$$\Phi_{SC} = \frac{kT_c}{e} \ln\left[\frac{n_c}{n_e - n_h}\right] \qquad (1)$$

where k is Boltzmann's constant, e is the unit electric charge, T_c is the cold electron temperature, n_c is the cold electron density from spectral fits assuming $\Phi_{SC} = 0$, n_e is the total electron density which is set equal to the ion density, and n_h is the hot electron density. Ion and electron measurements are not taken simultaneously. The ion data is linearly interpolated to obtain the total plasma density at the times when the electron measurements were taken. The

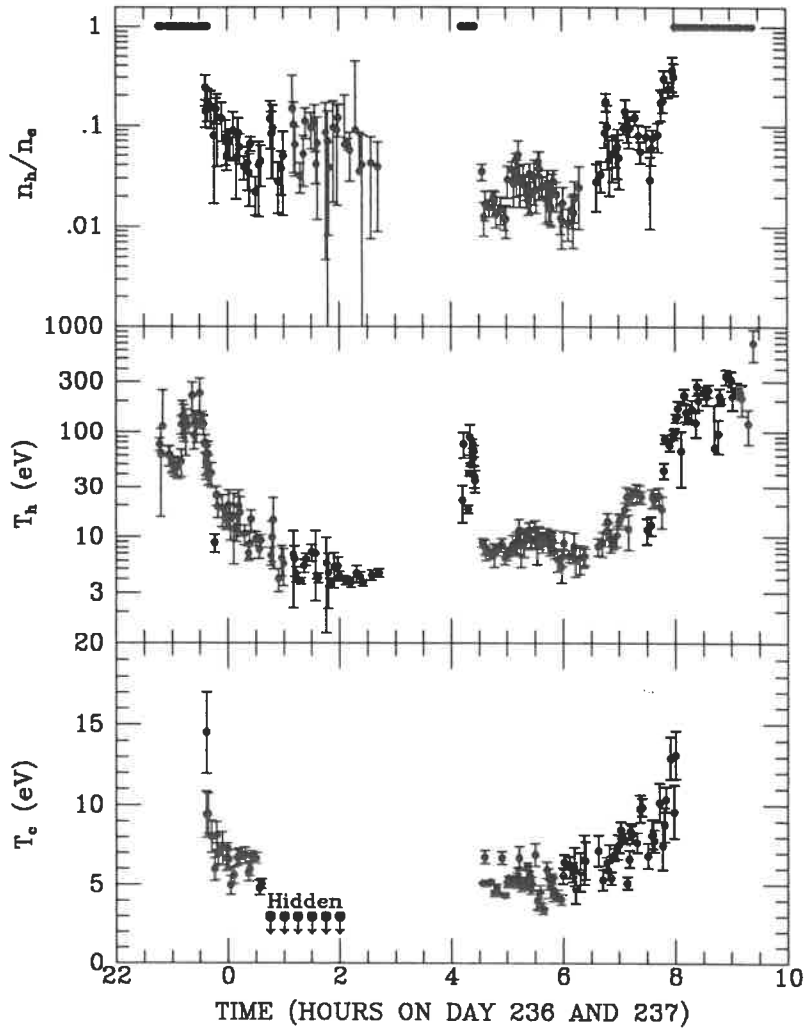

Figure 10. The temperature of the cold electron component (T_c), the temperature of hot electrons T_h, and the ratio of hot electron density to total electron density n_h/n_e. The data points labeled "hidden" are the upper limit for the cold electron temperature when the electron fluxes are below the instrument threshold.

hot electron density n_h is taken directly from the fits to the electron spectra as it is not affected by a small spacecraft charge.

Figure 11 shows the results of the calculation of the spacecraft potential Φ_{SC}. Also shown are 1σ error bars resulting from uncertainties in the ion densities, cold electron densities, and cold electron temperatures. As expected, the spacecraft potential is generally small in magnitude, less than 20 V negative.

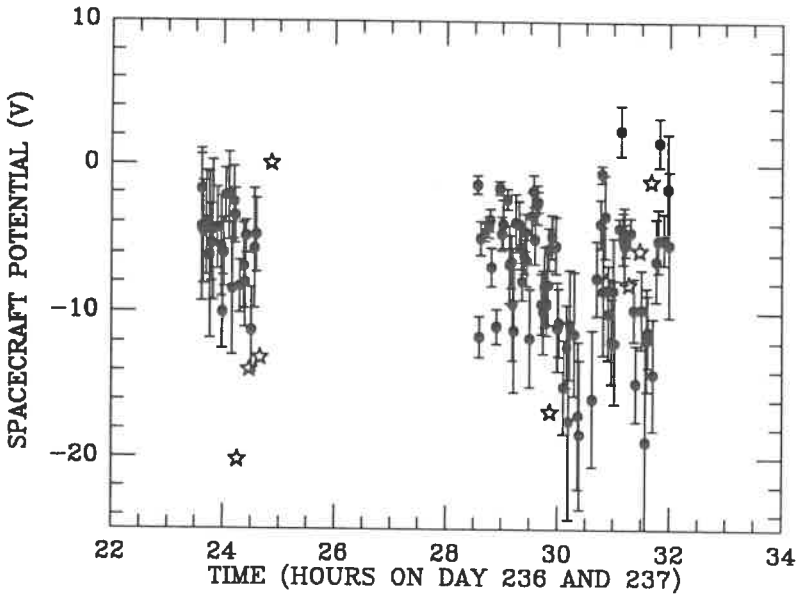

Figure 11. The inferred electric potential of Voyager 2 with respect to the ambient plasma while the spacecraft was within the magnetosphere of Neptune. Dots show the potentials and 1σ error bars derived from a comparison of ion and electron data and stars show the potentials derived using only ion M mode data.

The spacecraft potential can be determined independently using only the ion measurements. Figure 9 shows that ions generally appear to be super-corotational in the regions near the magnetic equator crossings at 0022 UT and 0755 UT on day 237. But the plasma beta value is small in Neptune's magnetosphere (Krimigis et al. 1989,1990), the corotation speed dominates the convection speed at Neptune (Selesnick 1990), and the effect of adding plasma would be to slow, not increase, the rotation rate: thus super-corotation of the plasma is not expected. The most plausible explanation of the apparent super-corotation is that the spacecraft had a negative charge, which accelerated positive ions into the PLS detector. The spacecraft potential would account for the difference between the energy of the ions observed by the detector and the corotational energy. The potential derived in this manner using the high-resolution M mode spectra are shown by stars in Fig. 11. Given the expected uncertainties, the spacecraft potentials determined independently via these two methods agree quite well, particularly in the outbound time period.

5. Plasma Distribution. Figure 12 shows the Voyager 2 trajectory in L shell versus time using the I8E1 model (Connerney et al. 1991). This figure also shows the radial distance and longitude; the brief intervals where L is less than R result from the higher-order moments of the field and can be thought of as due to the offset of the magnetic field from the center of Neptune. The large divergence of L from R in Fig. 12 indicates that plotting plasma parameters versus L will give a different result from plotting versus radial distance, particularly near closest approach inbound, where the spacecraft is at high magnetic latitudes.

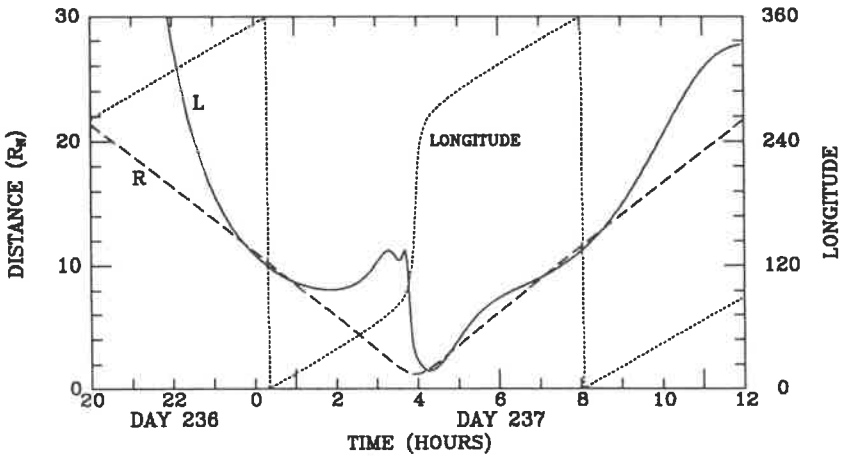

Figure 12. The spacecraft trajectory in L shell (solid line), radial distance (dashed line), and longitude (dotted line) plotted versus time.

This trajectory provides the opportunity to compare densities and temperatures at different latitudes and longitudes on the same L shell. Figures 13 and 14 show the H^+ and N^+ densities and temperatures plotted versus L shell using different symbols to indicate sweeps of the same L shells. Although the scatter is large, the densities in the region between L=8 and L=11 are comparable for all three passes through this region, except for the decrease in density inbound between L=8 and L=8.7. The N^+ density decreases with increasing L throughout this region, while the H^+ profile exhibits local maxima at $L\approx1.5$, $L\approx3$, and $L\approx8$ (inbound data) or $L\approx9$ (outbound data).

Plotting versus L shell also organizes the ion temperatures well. The H^+ temperatures are approximately the same during each crossing of these L shells, with the exception of the region just outside L=8 and at the high-latitude points between L=10 and L=12. A minimum in the H^+ temperature occurs at about L=8.5. The N^+ temperatures are also well organized by this scheme except, as with the H^+, in the region just outside $L\approx8$. The N^+ temperature decreases with increasing L throughout the magnetosphere.

The similar densities observed in all three regions indicate that the plasma is roughly isotropic over the longitude range sampled. If the plasma were anisotropic with $T_\perp > T_\parallel$, the magnetic mirror force would act to confine the plasma to the equator and the density would decrease with latitude. We note that the range of longitude covered by this conclusion is small ($<120°$), so that predicted longitudinal asymmetries (Broadfoot et al. 1989; Hill and Dessler 1990; Richardson et al. 1990) cannot be ruled out. In fact, the discrepancy

shock can be calculated. Upstream from the shock, the magnetosonic Mach number has a minimum value of 8.95, so the Neptunian bow shock can be characterized as a high Mach number, low to medium β, quasi-perpendicular shock. Other Mach numbers, both upstream and downstream of the shock, are tabulated in Table I.

In the MHD description above, we assumed that changes in plasma parameters across the shock are discontinuous. This is a crude approximation which breaks down when the small scale structure of the shock is investigated. The microstructure of bow shocks observed by the ISEE spacecraft has been studied in great detail at Earth and is consistent with current theories (Tsurutani and Stone 1985; Scudder et al. 1986*a*, *b*, *c*). The time resolution of the magnetic field measurements is much higher than that of the plasma measurements; therefore, scale sizes of the various microstructures are identified with greater accuracy from the magnetic field data. The magnetic field begins to increase at 1426 UT, approximately 10 min before the sharp transition (the ramp) at 1436 UT. This slow increase is called the foot of the shock. Because the spacecraft moves at 16.2 km s^{-1} along the shock normal and the shock moves toward the spacecraft at 15±12 km s^{-1}, the size of the foot should be 18,500±5400 km. The upstream foot of a perpendicular shock is attributed to the presence of ions which are reflected at the shock (Paschmann et al. 1982). One would expect the width of the foot to be a fraction of the effective ion gyroradius (a gyroradius is the radius of the trajectory a particle follows as it moves around a magnetic field line), $r'_{gi} = U/\Omega_{ci}$, which is 31,400±4000 km for the ions observed by PLS (see Table I). Here U is the relative speed between the solar wind and the bow shock along the shock normal and Ω_{ci} is the ion cyclotron frequency. For a perpendicular shock, Schwartz et al. (1983) derive a foot width of 0.7 r'_{gi}. This gives a foot width of 22,000±2800 km at Neptune, within 1σ standard deviation of the measured value.

Past the foot, the magnetic field increases rapidly to a maximum value $B_{\max}$ of 0.80±0.05 nT, then oscillates about the average downstream value of $B_d \approx 0.54 \pm 0.05$ nT. This gives a value for the overshoot $O \equiv (B_{\max} - B_d)/B_d$ of 0.48±0.07. This value of the overshoot is close to those of similar Mach number, low β, perpendicular and quasi-perpendicular shocks observed at Venus, Earth and Jupiter (Bagenal et al. 1987) and is in good agreement with the theoretical model predictions of Leroy (1983) for low β perpendicular shocks. The duration of the ramp was about 5 min, corresponding to a distance of 8700±2200 km. Theoretical studies suggest that the ramp should have a width equal to the ion inertial skin depth c/ω_{pi} (Schwartz 1985), where c is the speed of light and ω_{pi} is the proton plasma frequency. (The plasma frequency is the natural frequency at which the plasma oscillates and is proportional to the plasma density.) The width of the ramp at Neptune appears to be on the order of 2 ion inertial skin depths (see Table I), much thicker than the $0.2c/\omega_{pi}$ ramp width observed at Uranus (Bagenal et al. 1987).

The magnetic field magnitude dropped to much lower values after the overshoot and started a damped oscillation about the average downstream

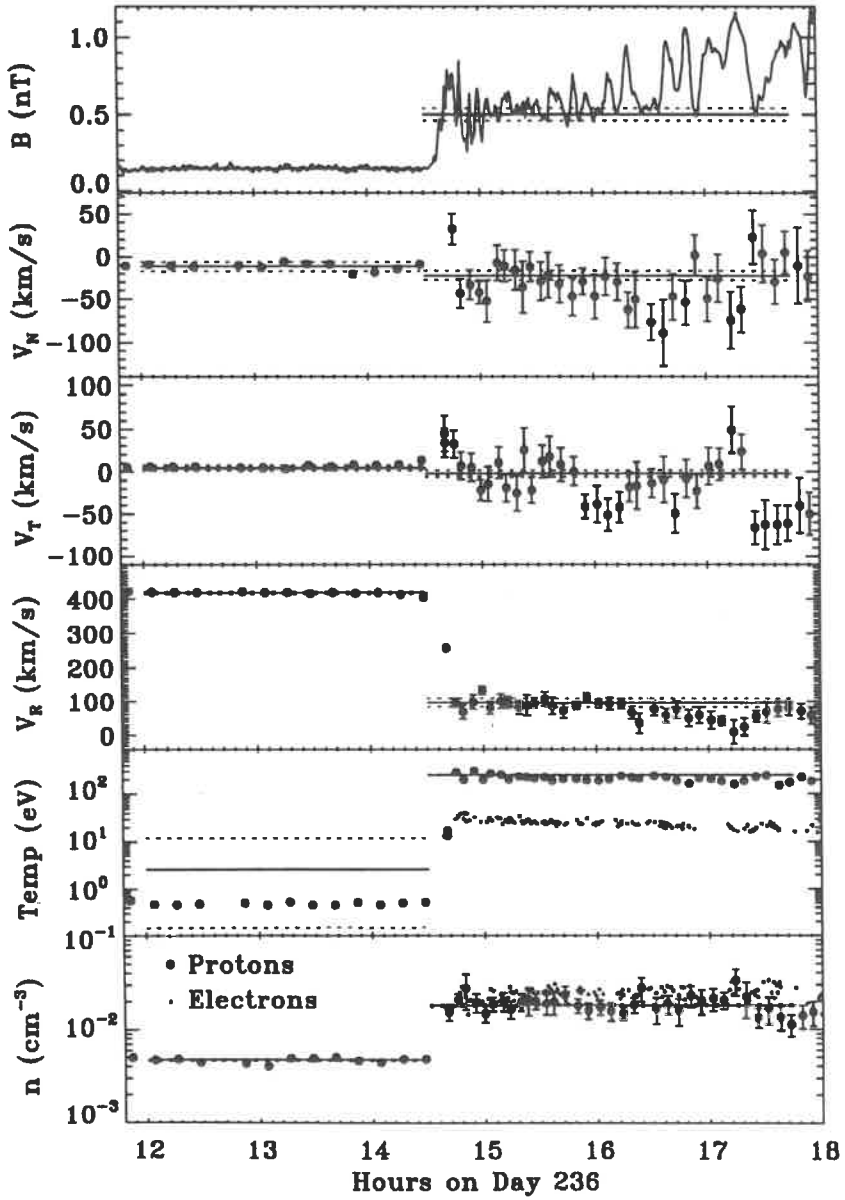

Figure 4. Voyager 2 measurements of the magnetic field magnitude, plasma bulk velocity, and electron and ion number densities and temperatures across the Neptunian bow shock. The solid lines represent the best solution of the Rankine-Hugoniot problem.

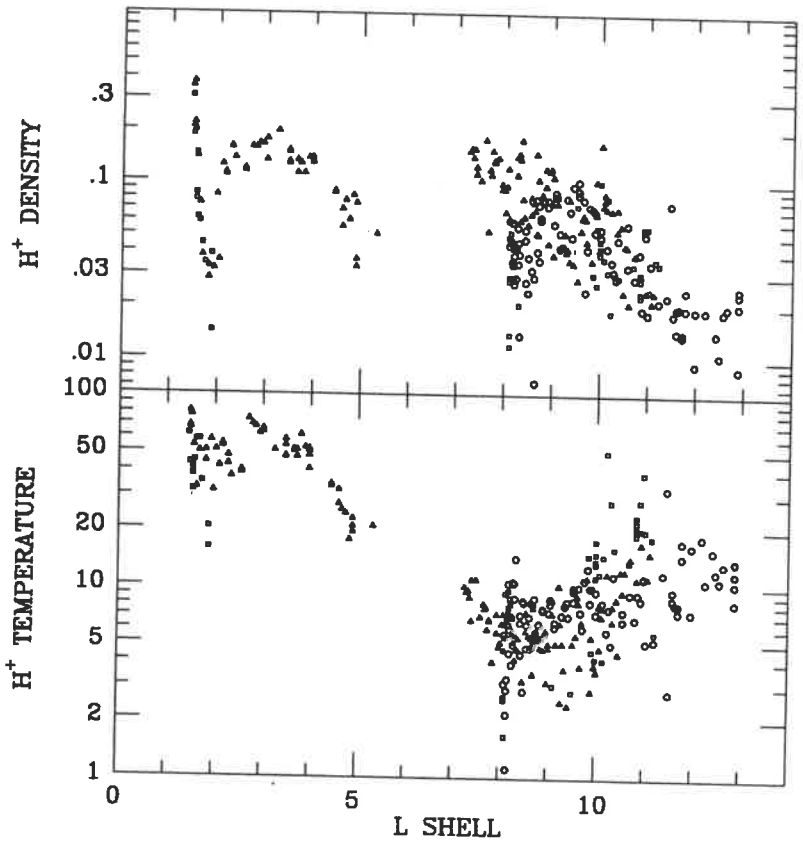

Figure 13. The H^+ densities and temperatures as a function of L shell. Open circles show data acquired inbound before the first minimum in L at 0055 UT on day 237, solid circles show data acquired a between this minimum and closest approach, and triangles show data obtained outbound.

between the inbound and outbound passes near L=8 may be due to either longitudinal asymmetry or plasma anisotropy; limited data coverage prevents us from drawing definitive conclusions. For most of the flyby pass, the temperatures are roughly consistent with the assumption that the plasma is isothermal along the magnetic field lines. This isothermal structure implies thermal isotropy of the local plasma distribution functions.

B. Conserved Magnetospheric Parameters

1. Flux Shell Content. When magnetic flux tubes move radially, the plasma moves with them. During these motions the quantity NL^2 is conserved, where N is the flux tube content, defined as the number of particles in a flux shell of unit width. Because NL^2 is conserved by diffusive and convective transport, locations of maxima and minima in NL^2 indicate the locations of

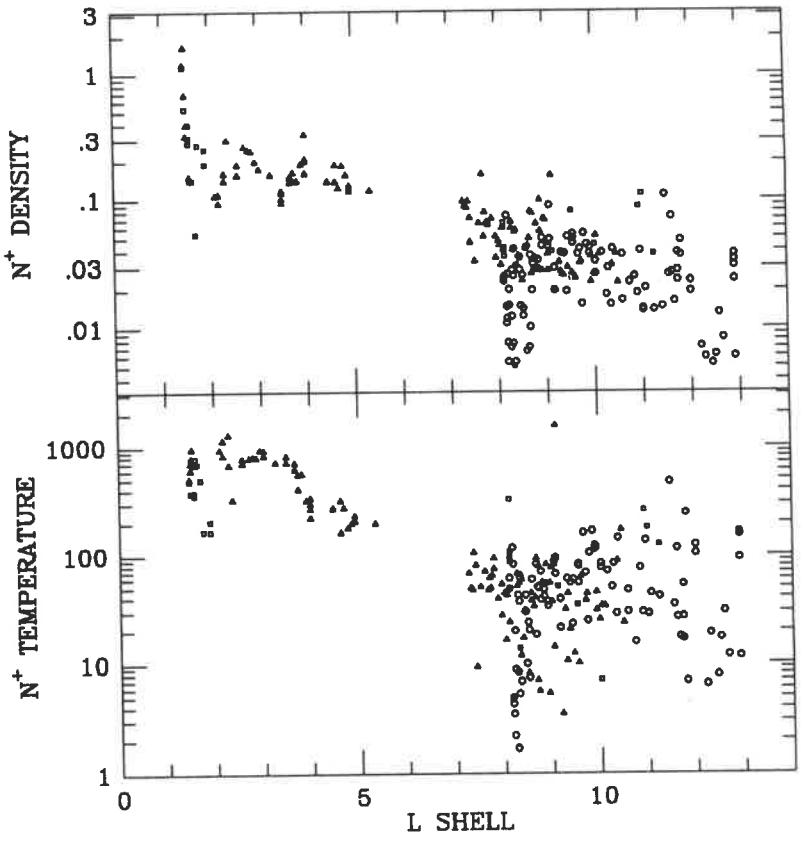

Figure 14. The N^+ densities and temperatures as a function of L shell. Open circles show data inbound before the first minimum in L at 0055 UT on day 237, solid circles show data between this minimum and closest approach, and triangles show data obtained outbound.

plasma sources and sinks. To derive the NL^2 values, the plasma density are first extrapolated along the magnetic field lines, then summed in latitude and longitude. The equation of force balance parallel to the magnetic field governs the plasma density distribution along a magnetic field line (Vasyliunas 1983),

$$\frac{\partial P_\parallel}{\partial S} - (P_\parallel - P_\perp)\frac{1}{B}\frac{\partial B}{\partial S} - n_i m_i \frac{\partial}{\partial S}\left[\frac{1}{2}\Omega^2\rho^2\right] +$$

$$n_i \frac{\partial}{\partial S}\left[\frac{GM_N m_i}{r}\right] + n_i Z_i q \frac{\partial \Phi}{\partial S} = 0. \qquad (2)$$

The first term is the pressure gradient force, where S is distance along a field line. The second is the force due to the magnetic mirror effect, which is zero unless the plasma is anisotropic. The third term is the centrifugal

force, where ρ is the distance from the planetary spin axis, Ω is the rotation rate of the plasma, and m_i and n_i are the mass and number density of each species i. This force pushes the plasma outward along field lines and thus toward the centrifugal equator. The next term is the gravitational force, where G is the gravitational constant and M_N the mass of Neptune. This term is only important close to the planet, as it is small compared to the centrifugal term outside synchronous orbit (R_{SYNC} is 3.372 R_N using a rotation period of 16.11 hours [Warwick et al. 1989] and $GM_N = 6.835$ km^3 s^{-2} [Tyler et al. 1989]). The last term is the force exerted by the ambipolar electric potential (Φ) set up by the interaction of plasma components of different masses m_i and charges $Z_i q$. Each ion and electron component requires an equation of the form of Eq. (2). The resulting set of equations is closed using the condition of charge neutrality, i.e., $\sum_i Z_i n_i = 0$.

In the Io torus (Bagenal and Sullivan 1981) and in Saturn's magnetosphere (Richardson and Sittler 1990), Eq. (2) has been solved assuming a dipole field geometry. The magnetic field at Neptune has large nondipolar components which contribute significantly to the magnetic field in much of the region sampled by Voyager. Therefore, to calculate NL^2 we integrate numerically along the magnetic field lines as described by the I8E1 magnetic field model of Connerney et al. (1991). We assume the plasma distribution functions are isotropic, i.e., that $P_\parallel$=$P_\perp$, so that the pressure gradient term in Eq. (2) vanishes; as we discuss later this is probably not true close to Neptune, but the effect on the results should be minor. We use a constant electron temperature of 10 eV in these calculations; the results are not sensitive to this parameter. In regions where data must be extrapolated to the equator from a high magnetic latitude the possibility exists that a particle population confined to equatorial regions could be missed. We consider this unlikely, as no signature of such a population was observed at any of the three crossings of the magnetic equator. Figure 15 shows profiles of NL^2 for H^+, N^+, and their total (which by assumption equals the electron NL^2 profile) as a function of L shell. Values for NL^2 are shown only at locations where both H^+ and N^+ densities and temperatures could be derived. The NL^2 profile for H^+ has a broad peak between $L\approx$8 and $L\approx$10. The N^+ and total ion profiles increase with L to the end of the data at L=13. The average value of NL^2 is 5×10^{31} for H^+ and 3×10^{31} for N^+ in this region. Inside L=7, NL^2 decreases rapidly for both ion species until just after closest approach, where the profiles of both species have a narrow peak. This increase near the minimum L shell (L_{min}=1.49 at 0417 UT on day 237) could be an artifact due to uncertainties in the magnetic field configuration or could indicate a plasma source close to the planet, or both. It corresponds to the narrow region of hot plasma near the crossing of the magnetic equator at 1.63 R_N (from 0406 to 0425 UT). Except for this increase, both the N^+ and H^+ profiles suggest that the plasma source is outside L=7. The H^+ source appears to be largest between L=8 and L=10, although it may extend over a large range of L shells. Similar reasoning implies the N^+ source is at or beyond the end of the available data (L > 13). The [illegible]

of the H^+ peak close to magnetic equator crossings (L=10.2 inbound and L=11.3 outbound) at first glance suggests that this peak could be a latitudinal effect. However, the higher-energy ions measured by the low-energy charged particle experiment also have a phase space density peak in this region (Cheng et al. 1991), which, combined with theoretical reasons to expect a peak in this region (see below), lead us to believe this is probably not a latitudinal effect.

The inbound and outbound values of NL^2 are nearly equal where they overlap between L=8 and L=10.5. These data were acquired between latitudes of 0° to 70° inbound and 0° to 19° outbound and longitudes of 354° to 77° inbound and 320° to 353° outbound. This similarity of the inbound and outbound NL^2 values is consistent with the assumption of isotropy.

2. *Energy Invariant.* Compression and expansion of the magnetic flux tubes due to radial motions result in adiabatic heating and cooling of the plasma. The quantity λ=$KV^{2/3}$ is conserved by this process, where K is the average energy of the plasma and V is the flux tube volume per unit magnetic flux (Selesnick and McNutt 1987). Figure 16 shows the quantity λ for H^+ and N^+. The value for H^+ decreases inward to L=8, remains constant between L=4 and L=8, and again decreases rapidly inside L=4. For N^+, λ has a large scatter, especially at large L, but is essentially constant from L=13 into L=3, inside which the value decreases. For each ion species, the inbound and outbound values of λ are approximately equal.

The implications which we draw from the plot of the energy invariant are similar to those from the NL^2 plot. The decrease in λ inside L=4 indicates that both H^+ and N^+ have energy sinks in this region. The constant value of λ for N^+ from L=13 in to L=4 indicates no N^+ energy sources or sinks are present in this region, consistent with a source outside L=13 as suggested by the NL^2 plot. The decrease in λ for H^+ from L=13 to L=8 is suggestive of an extended H source throughout this region; as the energy of a new ion roughly equals the corotation energy which is proportional to L^2, an increase of λ with L might be expected in this situation.

3. *Implications for Ion Composition.* We return briefly to the question of composition in the inner magnetosphere, where the spectra could be fit assuming the hot ion was either H^+ or N^+. Assuming the ion was N^+ gives NL^2 and λ profiles in the inner magnetosphere which appear to be continuations of those in the outer magnetosphere and are similar to those for the thermal H^+ component. The values of density and temperature are consistent with those expected if the N^+ in the outer magnetosphere is transported inward. If these ions are H^+, another source of hot H^+ is required near L=5; we can think of no source mechanism which would create large amounts of hot H^+ at this distance. Protons created this close to Neptune have a pickup energy of a few eV or less; large-scale energization would have to occur to bring them up to the observed energies. Thus, this circumstantial evidence strongly argues that the hot ions in the inner magnetosphere are N^+ from Triton.

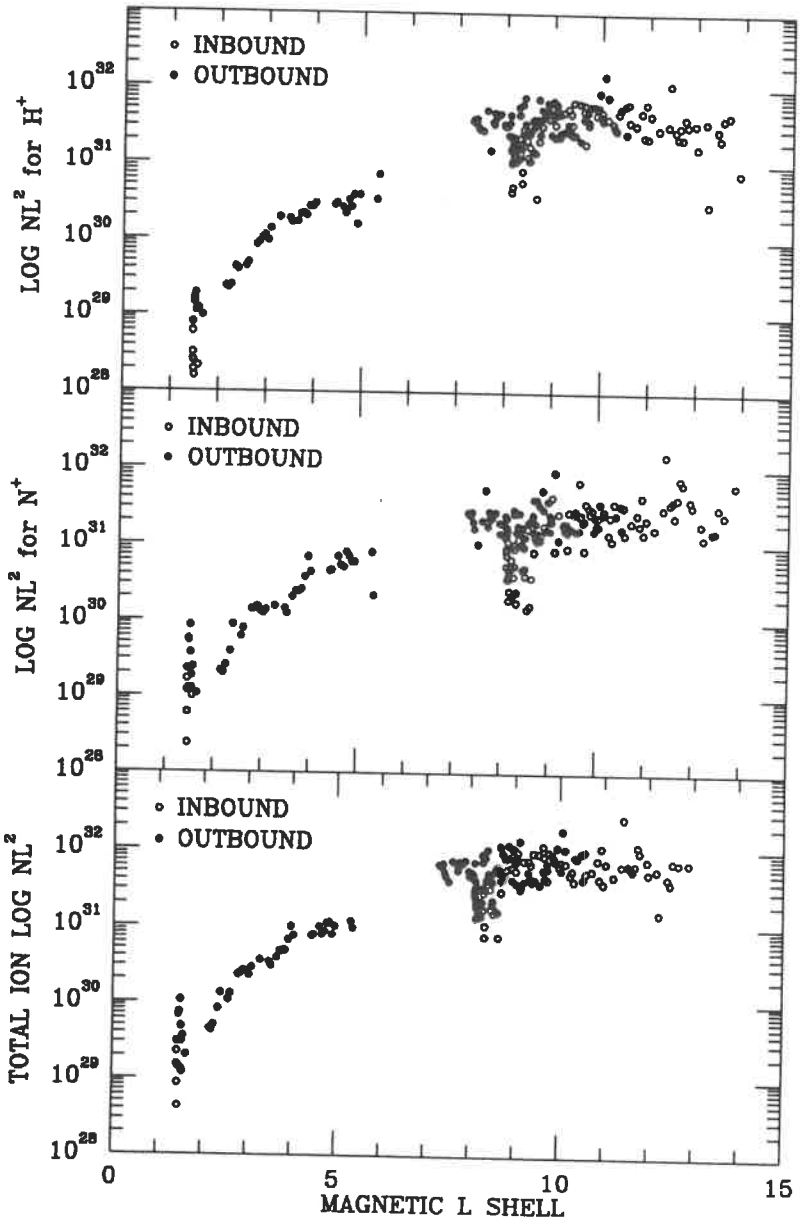

Figure 15. Profiles of the total flux shell content, NL^2, for H^+, N^+, and electrons.

C. Did Voyager 2 Enter Neptune's Ionosphere?

Voyager 2 approached Neptune more closely than any planet since it left Earth twelve years before. The inference of large plasma densities near

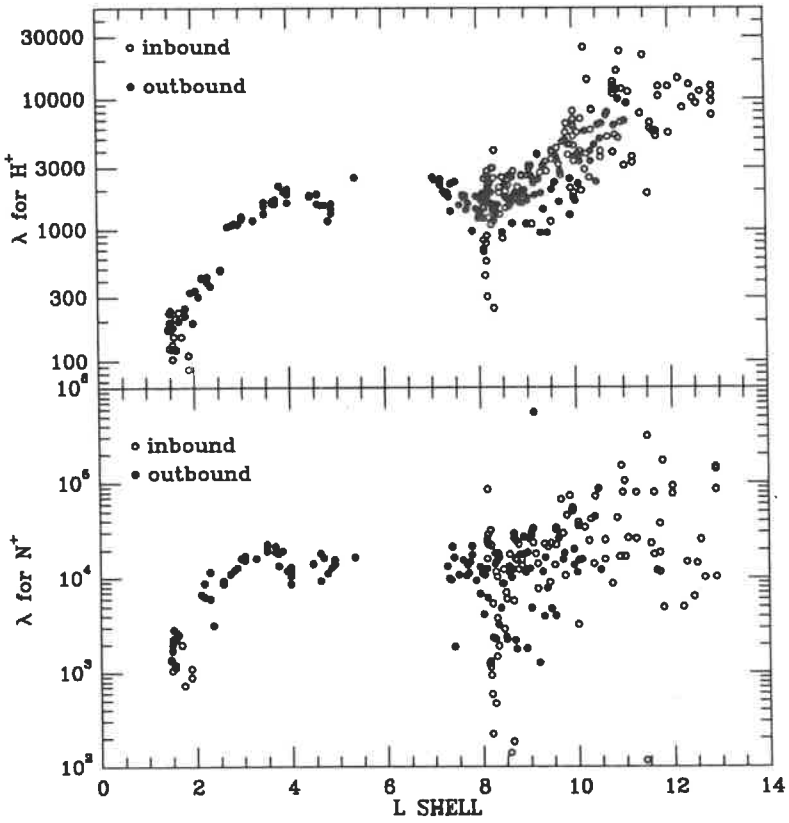

Figure 16. The energy invariant, λ, as a function of L for H^+ and N^+. This quantity would be a constant if transport were adiabatic.

closest approach from plasma wave and ionospheric measurements raises the question of whether Voyager entered Neptune's ionosphere, and, if so, was this plasma detectable by the PLS experiment. Gurnett et al. (1990) report the apparent observation of whistler waves between 0405:35 UT and 0425:30 UT on day 237 as Voyager moved from 1.30 R_N to 1.99 R_N from the planet. Whistlers are plasma waves which, at least at Earth, are generated by lightning in the atmosphere and move along magnetic field lines through the magnetosphere. The whistlers observed at Neptune exhibit unusually large dispersions (the wave frequencies observed decrease slowly with time); large dispersions are caused by waves moving large distances through regions of high plasma density. The region in which these whistlers are observed includes the period 0417 to 0424 UT in which relatively large plasma fluxes were observed. The maximum density observed with the PLS experiment of 2 cm^{-3} is in this region. Gurnett et al. (1990) note that the observation of whistlers is in direct conflict with the PLS plasma densities, which yield

electron plasma frequencies below the whistler frequencies. Even for very high ionospheric densities, larger than those observed by Tyler et al. (1989) by a factor of 300, they find that the required path lengths the whistlers must travel to produce the observed dispersions are very long, approximately 50 planetary radii. Plasma noise is also detected from 0405 UT to 0425 UT; Gurnett et al. (1990) argue that this noise is propagating in the whistler mode and thus sets a lower limit on the electron plasma frequency, and hence the electron density. From their plate A1, this noise reaches a maximum frequency of ≈45 kHz at ≈0410 UT and then monotonically decreases to ≈10 kHz at the end of this time period. If this noise is interpreted as being at the *in situ* electron plasma frequency, lower limits are set for the electron density of 25 cm^{-3} at 0410 UT, decreasing to 1.2 at 0425 UT. Gurnett et al. (1990) also argue that the observation of electrostatic $(n + 1/2) f_{ce}$ waves by Sawyer et al. (1990) from 0418 UT to 0422 UT suggests ambient electron densities of 500 cm^{-3} or more if these waves are associated with the upper hybrid resonance. Radio emissions reported by Kurth et al. (1990) suggest a density of at least 39 cm^{-3} at 0350 UT, a time at which no signature is observed in the PLS data (see Plate 6).

1. An Ionospheric Model. We expect the ionospheric density profile at closest approach to be similar to that probed by the radio science investigation (Tyler et al. 1989). Suppose that the ionosphere is isothermal and define the parameter λ by

$$\lambda \equiv \frac{GM_N m_p}{kT} \frac{1}{r} \tag{3}$$

where T is the temperature of the ionospheric plasma, m_p is the proton mass (H^+ is assumed to be the dominant ion), r is the distance from the center of Neptune, and the other symbols have their usual meanings. Then it can be shown that the ionospheric density $n(\lambda[r])$ varies as (see, e.g., Chamberlain 1963)

$$n(\lambda) \approx n_0 e^{\lambda - \lambda_0} \tag{4}$$

where the subscript 0 refers to a reference level and $\lambda_0 = r_0 H_0^{-1}$, where H_0 is the (isothermal) scale height at the reference level. From Tyler et al. (1989) we take n_0 = 1000 cm^{-3}, H_0 = 1800 km, r_0 = 1.068 R_N [these numbers are based upon (i) the definition that 1 R_N≡24, 765 km, (ii) the reference being 2000 km above the 1 bar level, and (iii) the 1 bar level taken as 24,450 km from Neptune's center at ≈60° latitude, from Fig. 3 of Lindal et al. (1990)]. On the basis of Eq. (4), the ionospheric density would be 245 cm^{-3} at closest approach and vary from 73 cm^{-3} down to 1.1 cm^{-3} during the period from 0405 UT to 0425 UT.

At this time the PLS instrument was oriented to observe precipitating particles, not corotating flow; despite this, we attempt to place limits on the maximum cold plasma density which could have been encountered locally during the whistler observations. The period from 0406 UT to 0425 UT is actually marked by fairly large PLS signals from the hot plasma encountered near the crossing of the magnetic equator which can "mask" signals from a colder plasma. For ionospheric plasma temperatures of 2 eV (proton thermal speeds of 20 km cm^{-3}), ionospheric (proton) densities of less than 720 cm^{-3} (0410 UT) down to 240 cm^{-3} (0425 UT) cannot be excluded by PLS data. However, the limiting density is a very rapidly varying function of the assumed temperature; at 0425 UT a proton temperature of 1.3 eV would allow a local proton density of 40, 000 cm^{-3} to be hidden from the PLS instrument. The answer to the question asked at the beginning of the section is that PLS did not detect ionospheric plasma, but neither can it place stringent upper limits on the amount of cold plasma in the region near closest approach. The limits for the plasma density set by PLS are consistent with models of whistler ray paths through the magnetosphere (Menietti et al. 1991). Whether Voyager 2 directly entered the ionosphere and the nature of the various wave emissions detected just after closest approach remain unsolved questions.

V. THE OUTBOUND MAGNETOSHEATH AND PLASMA MANTLE

Voyager crossed the magnetopause outbound from Neptune at 0819 UT on day 238, exiting the magnetotail and entering the magnetosheath. Figure 17 shows the three components of velocity, the density, and the temperature in the magnetosheath using the RTN coordinate system described earlier (Sec. III.A). Figure 18 shows the magnetic field components in the same coordinate system. The smooth curves superimposed on these data are the predicted variations in these quantities based on the magnetohydrodynamic model of Spreiter and Stahara (Richardson et al. 1994). This model is the most sophisticated available for simulating magnetosheath flow and has a record of success in simulating flow at other planets. The solar wind conditions just after the bow shock crossing outbound and a value for γ, the ratio of the specific heats, of 2 were used in this model to produce the curves shown in Figs. 17 and 18. The model matches the general sense of the plasma data well. Differences between the measured and the model values indicate departures either from the assumed solar wind parameters or from the assumptions of the gas-dynamic model.

Zhang et al. (1990) show that features in the magnetosheath data centered at 1700 UT on day 238 and 1000 UT in day 239 may be indicative of Voyager entering the plasma mantle. The plasma mantle is a region where the magnetic field is aligned with the field in the adjacent magnetotail, but which contains plasma from the magnetosheath. In this region magnetosheath plasma expands directly into the magnetosphere along open magnetic field lines and thereby determines important aspects of the magnetosphere's interaction with the solar wind (see, e.g., Coroniti and Kennel 1979; Siscoe and Sanchez 1987, and references therein). This region can be viewed as an expansion fan, beginning as a point in the front of the magnetosphere and expanding into the magnetotail and magnetosheath at the slow mode speed as it is convected anti-sunward. Thus the mantle region increases in size downstream from a

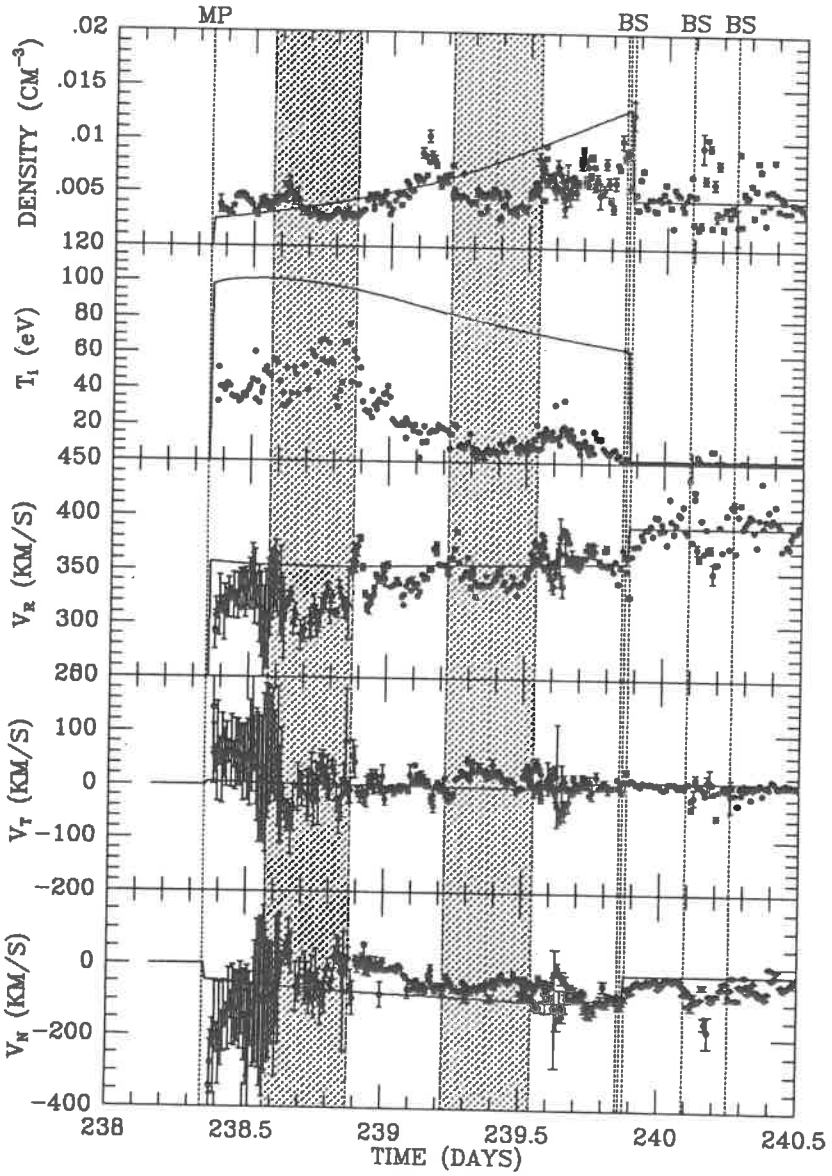

Figure 17. Plasma data obtained during Voyager's outbound magnetosheath crossing: number density (n), flow velocity (V_R, V_T, and V_N), and temperature (T_i). Smooth curves give baseline values from Spreiter and Stahara's model. Shaded regions correspond to the plasma mantle crossings.

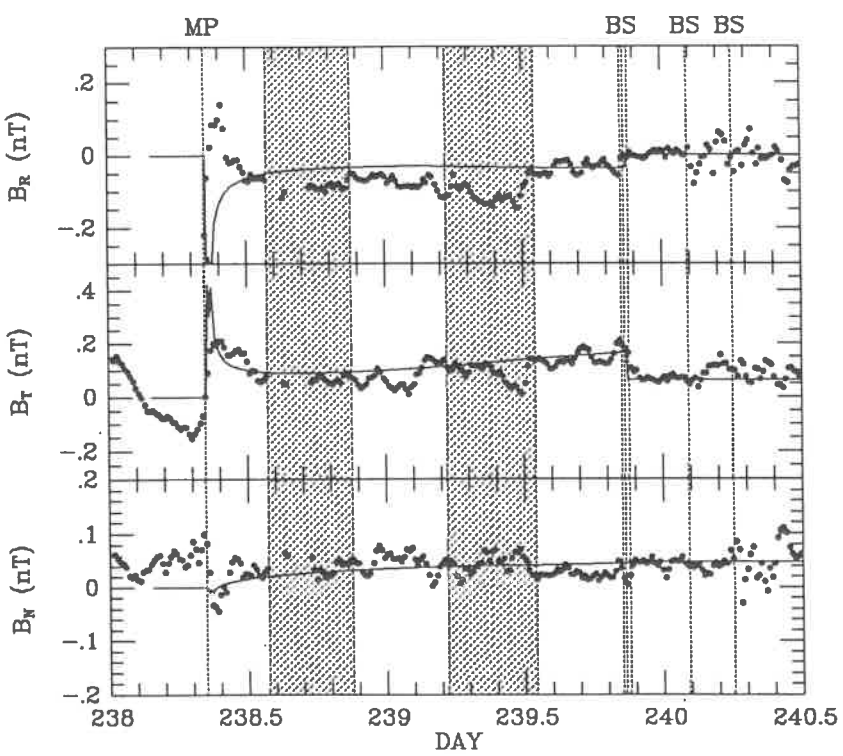

Figure 18. Components (B_R, B_T, and B_N) of the magnetic field data obtained during Voyager's outbound magnetosheath crossing. Smooth curves give baseline values from Spreiter and Stahara's model. Shaded regions correspond to the plasma mantle crossings.

planet; at Earth the plasma mantle fills a substantial fraction of the magnetotail at 80 Earth radii downstream (see, e.g., Hardy et al. 1975). Because the leading edge of the plasma mantle, which is a rotational discontinuity where the magnetic field direction changes from that determined by the draping of the interplanetary magnetic field (IMF) around the magnetosphere to that aligned with the magnetotail, propagates into the magnetosheath at an appreciable fraction of the Alfvén speed (the Alfvén speed is the speed at which magnetic waves propagate, $v_A \equiv B/\sqrt{4\pi\rho}$ where ρ is the mass density), the plasma mantle also expands into the magnetosheath. Before the Neptune encounter no observational evidence for this effect had been reported. Indeed, very few aspects of the plasma mantle or of the adjacent magnetosheath have been observationally studied, simply because their remote high-magnetic-latitude location has been beyond the reach of most spacecraft.

The magnetic field in the southern lobe of Neptune's magnetotail points toward the Sun, hence a field aligned with the magnetotail corresponds to zero B_T and a negative B_R in Fig. 18, whereas a draped, predominantly

eastward IMF produces a large positive B_T and small or negligible B_R. Aside from brief excursions, there are two intervals of large negative B_R and near-zero B_T; one centered near day 238.7 and one centered near day 239.4, one planetary rotation later. In both these intervals the velocity and density are reduced below the expected (model) values, a signature of the plasma mantle (Rosenbauer et al. 1975). The variations of the plasma and field parameters (except for the temperature) are thus consistent with the assumption that Voyager encountered the plasma mantle region during these two intervals. The temperature increases during the first putative mantle crossing and decreases during the other. Theory predicts a decrease in the temperature as the mantle plasma expands into the magnetosheath; however, all the near-Earth mantle entries shown by Rosenbauer et al. (1975) exhibit an increase in temperature at the crossing into the mantle from the magnetosheath. A better understanding of the nature of the mantle boundary is needed to properly account for the temperature signature. During the rest of the traversal, by contrast, the large positive B_T and small or near-zero B_R are consistent with the values expected from the draping of an eastward IMF, the velocity and thermal speed agree with their model values throughout and the density agrees with its model value throughout except near the end of the traversal. At this point the density and B_T undergo correlated quasi-periodic variations on a scale of a few hours for which we have no explanation at present (we note, however, that the ratio B_T/n remains nearly constant and equal to its model value during these variations, whereas during the assumed encounters with the plasma mantle the ratio is considerably higher than its model value, as expected).

We conclude that periodic encounters with the plasma mantle are the most likely explanation of the velocity, density, and temperature decreases and associated magnetic field changes observed during the Voyager outbound traversal of the magnetosheath at Neptune. This hypothesis implies that the plasma mantle extends considerably into the magnetosheath; the second encounter with the plasma mantle occurred when Voyager was 2/3 of the distance from the magnetopause to the bow shock. The second encounter is shorter than the first, consistent with this interpretation, but is farther out than predicted based on expansion of the mantle at the local Alfvén speed. However, the cusp at Neptune, from which the mantle emanates, lies in the sub-Alfvénic region of the magnetosheath. This may account for the mantle's large flare. (The attachment of the mantle to the cusp has yet to be worked out for Earth.)

VI. WAVES IN THE SOLAR WIND

Plasma waves in the solar wind that are associated with planetary bow shocks are a common phenomenon in the solar system. These waves are usually referred to as upstream waves, because they are generated in the regions upstream of the bow shock. They are often associated with energetic particles, which are either produced by acceleration processes at the bow shock or escape from the the magnetosphere (Scarf et al. 1970). Low-frequency electromagnetic waves with frequencies well below the proton cyclotron frequency are excited by upstream ions streaming along magnetic field lines through the solar wind plasma (Fairfield 1969; Barnes 1970; Gary et al. 1981). Upstream waves have been observed at Mercury by Fairfield and Behannon (1976); likewise at Venus by Hoppe and Russell (1981), Jupiter by Smith et al. (1976), Saturn (Behannon et al. 1985), Uranus (Russell et al. 1990; Zhang et al. 1991), and now Neptune (Zhang et al. 1991).

The last outbound bow shock crossing detected by the Voyager 2 spacecraft at Neptune was at 0900 UT on August 28, 1989 (Belcher et al. 1989; Ness et al. 1989). In the five days following this crossing, the interplanetary magnetic field (IMF) was only once oriented so that the spacecraft was magnetically connected to the bow shock. During this period, the spacecraft detected large-amplitude waves in the solar wind propagating away from the bow shock; these waves are almost certainly associated with Neptune. Figure 19 covers the 42-hr time period after the last bow shock crossing and provides an overview of the plasma and magnetic field data in the solar wind in this interval. The top two panels in Fig. 19 display the radial component of the solar wind velocity (V_R) and the radial component of the magnetic field (B_R). The upper two panels have 48 s resolution, the lower two show hourly averages of the magnetic field direction. The period where waves are observed is set off by the vertical bars. These waves are Alfvénic waves propagating at $\approx$140 ° to the ambient magnetic field and away from the bow shock. They have frequencies below the proton cyclotron frequency f_{cp}, which is about 10^{-3} Hz during the periods waves are observed. As at the other planets, these downstream waves are thought to be generated in the upstream region, where energetic protons created near the nose of the bow shock excite waves as they stream along solar wind magnetic field lines.

VII. THE MAGNETOSPHERE: INTERPRETATIONS AND MODELS

Returning to the magnetosphere proper, we note that although the plasma data suggests the locations of plasma sources and sinks, determining the magnitude of the source and the transport rate requires additional information. Models pertaining to the plasma source and transport mechanisms are summarized below.

A. Plasma Sources

Triton is probably the main source of plasma for Neptune's magnetosphere. Triton is the coldest object ever visited by a spacecraft, with an estimated daytime surface temperature of 38 K (Conrath et al. 1989) and an upper atmospheric temperature of 95 K (Broadfoot et al. 1989). Nonetheless, the Voyager 2 flyby of the Neptune system revealed a substantial ionosphere, with a classic Chapman profile and a density 10 times as large as the ionospheric density detected on Neptune itself (Tyler et al. 1989). Both ingress

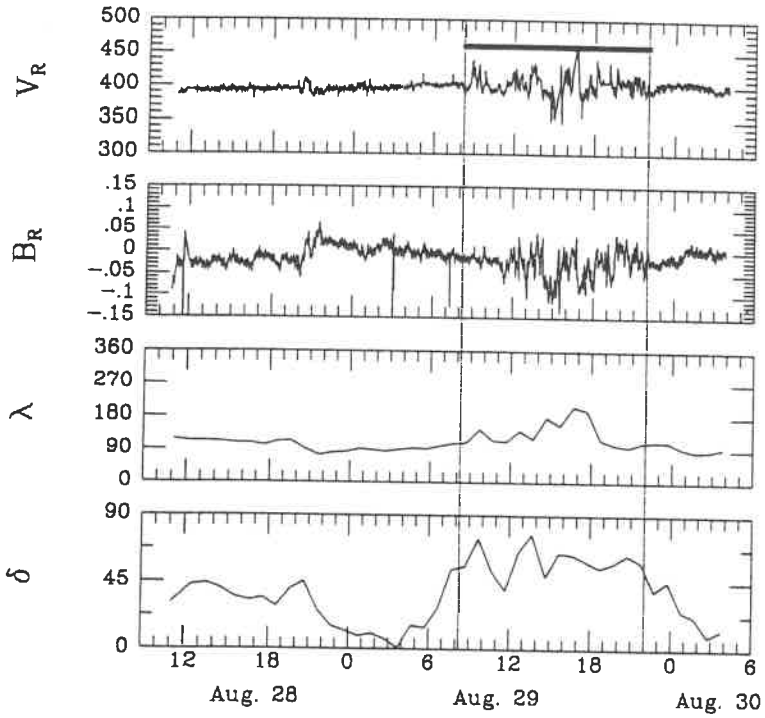

Figure 19. Overview of the solar wind plasma and magnetic field data outbound from Neptune. The direction of the magnetic field is represented by the north-south angle δ and east-west angle λ. The bold line shows the region where the spacecraft may be connected to the bow shock by the magnetic field.

and egress peaks detected by the Voyager radio science experiment occurred near 350 km, with peak densities of 2.3×10^4 cm^{-3} and 4.6×10^4 cm^{-3}, respectively. Although the dominant ion was originally suggested to be N_2^+, with a topside plasma temperature of 80°±16 K (Tyler et al. 1989), more detailed considerations have shown that N^+ or C^+ should be the dominant ion (Ip 1990; Yung and Lyons 1990; Lyons et al. 1992; Majeed et al. 1990; Summers and Strobel 1991).

Yung and Lyons (1990) find that dissociative recombination produces exothermic nitrogen atoms and N^+ with a total escape flux $\approx 8 \times 10^{24}$ s^{-1}. A recent revision of their model suggests that C^+ may be the dominant ion (Lyons et al. 1992); this is close enough in mass to N^+ that the PLS instrument could not tell them apart. Summers and Strobel (1991) find that more than 95% of the particles escaping Triton are neutral, with H escape determined by methane photolysis rates and N escape controlled by the energy deposition rate due to precipitating magnetospheric electrons. Their preferred escape rates are 7×10^{25} s^{-1} and 3.4×10^{25} s^{-1} for H and N, respectively. Strobel (personal communication) states that only the tail of the N distribution in Triton's atmosphere has enough energy to escape, so escaping N forms a neutral cloud tightly constrained to Triton's orbit. The H escapes with velocities of several km s^{-1} and thus can form an extended cloud. A recent model of this H cloud indicates that collisions between the neutral H atoms in the cloud may cause the cloud to extend throughout Neptune's magnetosphere (Decker and Cheng 1994). This model has not yet been used to determine the morphology of the N cloud.

The other possibly important plasma source is Neptune itself. We discussed earlier the possibility that large densities of cold plasma could reach the innermost magnetosphere from the ionosphere. Richardson et al. (1990) suggest that a neutral cloud of H from Neptune's atmosphere may be a sink for hot ions and energy and a source of cold ions via charge exchange. The charge exchange process involves an ion colliding with a neutral and gaining an electron from it. The initial ion is now a neutral atom and, as its velocity is usually greater than the escape speed, it leaves the Neptune system. The original neutral is accelerated to the corotation velocity when it is ionized and it gains an initial perpendicular temperature roughly equal to the corotation energy (actually, $E_i = \frac{1}{2} m_i (v_c - v_N)^2$, where v_N is the speed of the neutral when it was ionized). In the outer magnetosphere this has the effect of changing the temperature of the plasma while leaving the density the same. Near the planet, however, the corotation energy falls below the instrument's energy threshold of 10 eV, so the old ion is replaced by an undetectable ion, giving the signature of a plasma sink. The efficiency of this loss depends on the neutral density, the charge exchange cross section, and the plasma transport speed (because more plasma would be lost if it were moving slowly). In light of the recent work of Decker and Cheng (1994) showing that neutral H from Triton can populate the entire magnetosphere, a Neptune source of neutrals may not be required to explain the data.

B. Plasma Transport

The removal of plasma may take place via an organized convection system, by diffusion, or by *in situ* plasma losses such as charge exchange or recombination. Reaction rates are too small in the outer magnetosphere for *in situ* losses to be effective, so transport is an important loss mechanism. The transport rate must be fast enough to remove plasma at the same rate it is added to the magnetosphere to maintain a steady state. Because at least 10 to 20% of the neutrals escaping from Triton are ionized in the magnetosphere (Decker and Cheng 1994), the plasma source is at least 0.1 to 0.2 times the neutral source. A rough estimate of the transport time τ_T is given by N_i/S_i, where S_i is the ion source; for a source of of 10^{25} ions per second (15% of the H source) $\tau_T = 4 \times 10^4$ s, or about 13 hr, at Triton.

1. Convection Models. Two convection systems have appeared in the literature which may provide such rapid transport. Hill and Dessler (1990) suggest that longitudinally asymmetric mass loading, with peaks at the longitudes where Triton's orbit intersects the plasma equator (170° and 350°),

drives a four cell convection system with outward transport sectors centered on the longitudes of peak mass loading and inward transport elsewhere. The mass-loading is asymmetric because the plasma density decreases outward and the tilt of Neptune's magnetic dipole and Triton's orbit inclination combine to cause the L shell of Triton's orbit (and thus of the orbit of the neutral torus) to vary with longitude from 14.3 to over 50. The ionization rate of the neutrals peaks where the plasma density is highest, at longitudes 170° and 350° where Triton is at its minimum L shell. The Hill and Dessler (1990) model calls for the more heavily loaded flux tubes at those longitudes to move outwards due to the centrifugal force, with compensating inward motion at other longitudes

Selesnick (1990) suggests that the tilt of the dipole allows a solar wind driven convection system to operate by modulating the convection electric field on the time scale of the planetary rotation. The flow of the solar wind past the magnetosphere produces a convective electric field, $\mathbf{E} = -\mathbf{v} \times \mathbf{B}$, across the tail of the magnetosphere. This electric field causes plasma to move sunward. At planets with a rotational axis perpendicular to the solar wind flow and a small dipole tilt, the motion of plasma due to the electric field averages to zero, as inward plasma motion on the night side is matched by outward motion on the day side. Neptune, however, presents a different face to the solar wind every half rotation, going from a pole-on to Earth-like configuration. The coupling efficiency between the solar wind and the magnetosphere (which determines the magnitude of the convection electric field) varies with the angle between the dipole axis and the solar wind. Neptune's rotation therefore causes a sinusoidal variation of the convection electric field which drives the system like a forced harmonic oscillator, moving plasma outwards between longitudes 170° and 350° and inwards in the opposite hemisphere.

The data appear qualitatively inconsistent with either mechanism, but neither can be definitively ruled out because of low plasma fluxes in the vicinity of Triton's minimum L shell. As noted above, the Hill and Dessler model predicts maximum outflow at 170° and 350° longitude; both the inbound and outbound plasma sheet crossings occurred at about 350° longitude; the NL^2 profiles in each case indicated transport was inward. However, Hill and Dessler (1990) note that ring-current shielding may limit their convection system to the region outside Triton's orbital distance where the PLS data provide no constraints.

The Selesnick model predicts outflow between, rather than at, longitudes 170° and 350°. Voyager is in this longitude sector from $L \approx 10$ inbound to closest approach. In this region the NL^2 profiles indicate that transport is inward. Here the caveat is that Fig. 15, which shows NL^2 as a function of L, was constructed assuming azimuthal symmetry while the model of Selesnick (1990) has an inherent longitudinal asymmetry. In addition, the model effects are presumably most apparent near the plasma source, i.e., Triton's orbit. Thus, neither of these mechanisms fits the observations inside $L \approx 13\,R_N$, but neither can be ruled out in the Triton region. In either case, the convection speed is slow compared to the corotation speed and is too small to be directly determined from the PLS measurements.

2. *Diffusion.* The other form of transport occurring in planetary magnetospheres is diffusion. Diffusion of plasma results from stochastic changes in the magnetic or electric field on a time scale less than the time required for the plasma to move around the planet (i.e., the third adiabatic invariant is violated [see Schulz and Lanzerotti 1974]). The driving mechanism for plasma diffusion in Saturn's magnetosphere and for energetic particles at Uranus is probably atmospheric winds. Neutral winds which occur at ionospheric altitudes couple more efficiently to ions than electrons, producing electric fields in this region. Because magnetic field lines are equipotentials, these electric fields are transmitted to the magnetosphere. As the atmospheric winds change, so do the electric fields, causing stochastic changes in the particle trajectories and net radial motion of the plasma. This transport process results in motion away from the source region at all longitudes, consistent with the available data, but would require a diffusion rate much larger than that observed at other planets. For atmospheric-wind-driven diffusion, the diffusion coefficient $D_{LL} = D_0 L^3$, where D_0 is a constant (Brice and McDonough 1972; Coroniti 1974). Because $\tau_T \approx D_{LL}^{-1}$, for $\tau_T = 4 \times 10^4$s at L=10 we find $D_0 = 2.5 \times 10^{-8}\,R_N^2\,s^{-1}$. This is six times the rate at Jupiter and ten times the fastest estimate at Saturn. Thus the main conclusion is that plasma transport is very rapid, with plasma removal times of a day or less near L=10, but the mechanism is not yet determined.

C. Plasma Sinks

1. *Charge Exchange.* The NL^2 and λ plots (Figs. 16 and 17, respectively) both indicate that losses occur inside L=4. Three possible loss mechanisms are charge exchange, precipitation of ions into Neptune's atmosphere, and ring absorption. The charge exchange process is also a plasma source and is described above in the source section. For charge exchange to operate, a cloud of neutrals must be present; near the planet this could be due to an extended planetary atmosphere (Richardson et al. 1991) or neutrals from Triton that have been scattered via collision to orbits near to Neptune (Decker and Cheng 1994).

2. *Precipitation Losses.* Plasma cannot easily cross a magnetic field line but can move easily along the magnetic field. If plasma particles encounter the atmosphere, they will be lost through collision. This loss process creates a region of phase space parallel to the magnetic field, called the loss cone, which is devoid of ions due to atmospheric losses. The size of this loss cone increases near the planet due to the geometry of the magnetic field lines, so the percentage of the plasma which enters the atmosphere increases near Neptune. If plasma diffuses into the loss cone (because of wave-particle scattering, for example) the entire plasma population can be reduced in this manner. Figure 20 shows the size of the loss cone at the spacecraft position. Near closest approach it is as large as 40°, so a substantial portion of an

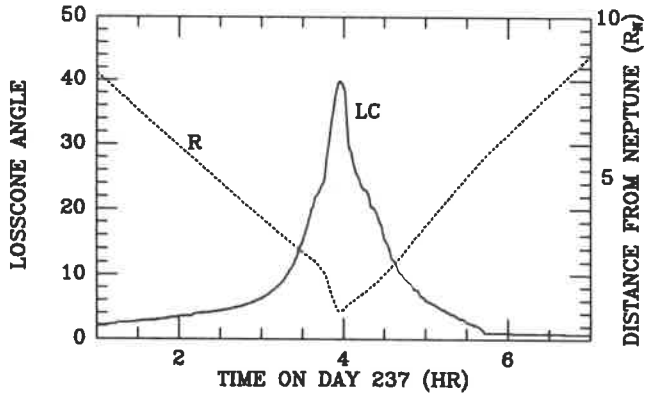

Figure 20. The loss cone angle (LC) at the spacecraft calculated assuming loss occurs at 1 R_N and using the I8E1 magnetic field model. Also shown is the distance of the spacecraft from Neptune, R, in Neptunian radii.

isotropic distribution would be lost.

The spectra in this region strongly suggest that precipitation losses are occurring. Near 0430 UT on day 237 the spacecraft and magnetic field orientations are such that the three sunward-looking cups (A, B, and C) view the plasma distribution perpendicular to the magnetic field and the fourth detector (D) looks approximately along the magnetic field direction. Figure 21 shows the ion currents measured in the C and D cups and the electron currents, plus information on ring locations and L shells which are described below. After 0415 UT the current observed in the C cup is larger than that observed in the D cup. As the electron and C cup fluxes are the same in this region, the cause must be a depletion of current in the D cup. This difference is nearly a factor of 10 at 0422 UT, then decreases to less than a factor of 2 by 0500 UT. Richardson et al. (1991) fit a set of spectra at 0420 UT; they show that an isotropic simulation gives too much current in the D cup; much better fits to the data are obtained using an anisotropy ($A = T_\perp/T_\parallel - 1$) of 11 for H^+ and 3 for N^+.

The cause of this apparent anisotropy is probably not a bi-Maxwellian distribution function but a loss cone distribution with a large cone angle. The angle between the magnetic field and the D cup look direction at 0420 UT is about the same as the loss cone angle (20°), so the flux observed in the D cup should be strongly affected by loss cone effects in this region. As the field direction changes further along the spacecraft trajectory so that the D cup is at a larger angle to the magnetic field, the difference between the fluxes observed in the C and D cups decreases.

The evidence that precipitation losses occur is compelling, given that the loss cone is empty. The total amount of plasma lost via this mechanism depends on the rate of pitch angle diffusion, i.e., how fast the loss cone is refilled. The maximum loss rate is called the strong diffusion limit, defined

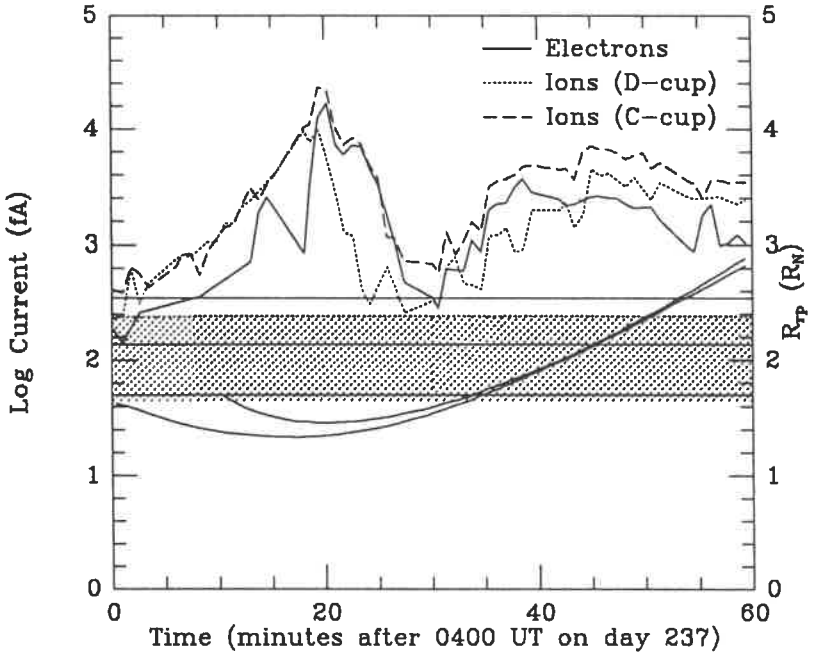

Figure 21. The PLS electron and ion currents for the time period from 237/0400 UT to 237/0500 UT. The two smooth curves show the radial distance of the ring plane intersection point of the magnetic field lines that pass through the spacecraft, using two different magnetic field models. The three horizontal lines represent the positions of Neptune's three major rings. The depletion of the currents at about 0430 UT corresponds to crossing of the inner (broad) ring, as indicated by the shaded region.

as having the loss cone refilled by pitch angle diffusion of the plasma as rapidly as it is emptied. Figure 21, which shows that ion flux parallel to the magnetic field is much smaller than that perpendicular to it, indicates that the loss rate is substantially below the strong diffusion limit. Various wave modes observed by the plasma wave (PWS) experiment on Voyager may be associated with precipitation and/or adiabatic inward diffusion of plasma from Triton (Barbosa et al. 1990). A fully consistent picture of what is happening in this region requires a synthesis of these diverse data sets.

3. Ring Absorption. During Voyager's flyby of Neptune, 6 small satellites and a ring system were discovered within 6 R_N of Neptune (Smith et al. 1989). The spacecraft went very close to Neptune; closest approach was only 0.2 R_N from the cloud tops. This deep penetration into the Neptunian system enabled PLS to detect a possible ring absorption feature in the plasma data.

Ring absorption and satellite sweeping signatures in charged particle data were reported during many previous planetary encounters (see, e.g., Van Allen et al. 1980; Simpson et al. 1980; Van Allen 1983; Krimigis and Armstrong

1982), but most of these signatures were observed in the high-energy particles. The absorption of low energy charged particles by satellites is very difficult to detect because the total absorption cross section of the satellites is much smaller than that of the rings and because the satellite absorption occurs over a very small range of L shells. Ring absorption of low-energy particles is easier to observe because the loss region covers a larger area. For the low-energy particles considered here, these signatures are observed only when the spacecraft and the ring are on the same magnetic field line. The detailed behavior of ring absorption depends upon the properties of the particles or dust that constitute the ring.

Again we refer to Fig. 21, which shows electron and ion currents measured by the PLS experiment during the hour after closest approach. The solid line is the electron current in the D cup, the dotted line is the ion current in the D cup, and the dashed line is the ion current in the C cup. The two smooth curves are the radial distance (R_{eq}) of the ring plane intersection point of the magnetic field line that passes through the spacecraft. Two different magnetic field models, the OTD model and the I8E1 field model, are used in the calculations. Although these magnetic field models are not reliable inside 4 R_N, they agree with each other quite well, implying that the calculation of R_{eq} is not sensitive to the field model chosen. If the distance R_{eq} is equal to the radius of a ring, the spacecraft is magnetically connected with that ring. The three horizontal lines indicate the locations of Neptune's three rings. A sheet of ring material (see Fig. 17 by Smith et al. 1989) extends from radius 1.65 R_N to 2.38 R_N, as indicated by the shaded area. In this region, fluxes detected by the PLS instrument are lower than in the surrounding regions. Because this feature is correlated with the location of the broad ring, we attribute this decrease to ring absorption. The ring 1989N1R does not produce such a feature, perhaps because it is so narrow.

Mauk et al. (1990) report that a feature in the low-energy charged particle (LECP) data at 0419 UT of day 237 is due to ring absorption, but this feature occurs 8 min. earlier than the decrease in the PLS data. This difference is not understood. The cosmic ray subsystem (CRS) data show a flux decrease between 0428 UT and 0442 UT (Stone et al. 1989), which is at roughly the same time as the decrease in the plasma fluxes. This decrease in the CRS fluxes is interpreted as an absorption signature of a combination of small satellites and rings (see also Selesnick 1992).

If the depletion in the fluxes near 0430 UT is due to ring absorption, we can estimate limits for the plasma transport time. The time scale for radial transport must be comparable to that for ring absorption in order for this feature to exist. We assume that the radii of ring particles are much smaller than the gyroradius of charged particles ($\approx$1 m). Then the time scale for ring absorption τ_a is (Zhang et al. 1991)

$$\tau_a = \frac{\tau_B \cos\chi}{2\xi \tan\alpha_0} \tag{5}$$

where τ_B is the bounce time, ξ is the optical depth, α_0 is the average particle pitch angle, and χ is the angle between the magnetic field lines and the normal to the ring plane. The bounce time τ_B is estimated to be 10^2 s for protons with kinetic energies on the order of 100 eV. The optical depth ξ is 10^{-4} (Smith et al. 1989). The quantity $\cos\chi/\tan\alpha_0$ is of the order 10^{-1} if the proton anisotropy A=11 as determined above. Therefore, the ring absorption time τ_a is about 10^5 s. Thus 10^5 s is the lower limit for the radial diffusion time. To estimate an upper limit, we note that hot plasma was observed inside the ring system in the PLS data (see Plate 6 and Figs. 6 and 7). Plasma of planetary origin would be cold (the ionospheric temperature is about 950 K (Tyler et al. 1989), so this plasma probably comes from outside of the ring. One possible mechanism for transport across the ring is for low-energy particles to diffuse in at longitudes where the ring is at high magnetic latitudes and spans a large range of L shells. At these longitudes only those ions and electrons with small pitch angles collide with the ring matter. The condition for mechanism to be viable is that the time scale for the gradient drift be longer than the radial diffusion time, an ordering that is generally the case for low-energy plasma. (Ions and electrons drift around the planet in longitude due to the radial gradient and curvature of the magnetic field. The direction of the drift depends on the sign of the charge and the speed on the particle energy.) For 1-keV particles (the temperature of the N^+ ions near closest approach [Richardson et al. 1991]), the drift time τ_{DB} at L=2 is 5×10^7 s. Thus the radial diffusion time for low-energy plasma at the location of the ring should satisfy 10^5 s$<\tau_a=D_{LL}^{-1}<10^7$ s. Using the D_0 value of 2.5×10^{-7} R_N^2 s^{-1} we found previously, we can evaluate D_{LL}, finding that $D_{LL} = 2 \times 10^{-6}$ R_N^2 s^{-1} at L=2. Then the diffusion time is 5×10^5 s, which is consistent with the above condition.

The absorption feature also allows us to calculate the diffusion coefficient quantitatively. The equation that governs the variation of the plasma density n in the absorption region is (Fälthammar 1968)

$$L^2 \frac{\partial}{\partial L}\left[\frac{D_{LL}}{L^2}\frac{\partial}{\partial L}(nL^4)\right] = -\frac{nL^4}{\tau_a}. \tag{6}$$

Using dimensional analysis, we estimate the absorption width ΔL from Eq. (6) and find that $\Delta L=\sqrt{\tau_a D_0 \overline{L}^3}$. Taking ΔL=0.3 and $\overline{L}$=2 from Fig. 21, we find that $D_0 = 1.1 \times 10^{-7}$ s^{-1}. This is within a factor of 4 of the previous result.

4. Magnetospheric Scenarios and Models. One scenario in the literature hypothesizes a large neutral cloud of H extending from 8 R_N out past Triton and a much narrower neutral cloud confined near Triton's orbit (Richardson et al. 1991; Zhang et al. 1991). This scenario is consistent with atmospheric models which predict that H escapes Triton's atmosphere with speeds of several km s^{-1}, allowing it to spread further than N, which barely has enough energy to escape from Triton (D. F. Strobel, personal communication). The source of H^+ would occur from L=8 outward and the source of N^+ would be near Triton for

N^+. One problem with this scenario is that all the neutrals produced by Triton would be ionized in the magnetosphere. Because ionization rates are low, an ion source of 10^{25} s^{-1} requires neutral densities of 300 to 600 cm^{-3}. Neutral H densities this large should have been detected by the UVS experiment (Cheng 1990) but have not been reported.

A possible solution to the large neutral density problem is provided by Decker and Cheng (1994) who use a Monte Carlo technique to follow neutral H which escapes from Triton. They find that the H density peak is about 60 cm^{-3} and is located at Triton. The ion source is only 15% of the neutral source; the remaining neutrals are ionized in the solar wind or are lost via collision with Neptune. This model assumes a total H source rate of 10^{25} s^{-1}; a larger rate, such as the 7×10^{25} s^{-1} calculated by Summers and Strobel (1991), would give larger densities. Models of the magnetosphere are used to test hypotheses concerning the physical processes and rates which occur in the magnetosphere. The purpose of this section is to present some of the methods used to model the magnetosphere of Neptune and show some simple results (see Richardson 1994). Many aspects of Neptune's magnetospheric plasma are not yet understood and are the focus of active research.

The chemistry and transport of plasma are combined in this section to produce a quantitative model of the magnetosphere which can provide a rough idea of the transport rates, plasma source, and neutral densities implied by the observations. The basic equations are those governing the transport of particles and energy,

$$L^2 \frac{\partial}{\partial L}\left[\frac{D_{LL}}{L^2}\frac{\partial N_i L^2}{\partial L}\right] + S_i - R_i = 0 \tag{7a}$$

$$L^2 \frac{\partial}{\partial L}\left[\frac{D_{LL}}{L^2}\frac{\partial N_i L^{14/3} T_i}{\partial L}\right] + S_i - R_i = 0 \tag{7b}$$

where D_{LL} is the diffusion coefficient and S and R are the source and loss rates, respectively. The diffusion coefficient is usually expressed in the form $D_{LL} = D_0 L^m$ where D_0 and m are constants. On the basis of empirical results from the other giant planets (Goertz and Thomsen 1979; Hood 1983,1985,1989*a*, *b*), we take m=3, which is the value expected for atmospherically driven diffusion (Brice and McDonough 1972; Coroniti 1974) and which we invoked earlier in the discussion of plasma transport. The energy diffusion equation is derived as in Richardson and Siscoe (1983), but differs from their result because the plasma is assumed to be spread uniformly along magnetic field lines rather than confined to the equator by the centrifugal force.

The plasma source is ionization of neutrals which escape from Triton. We use as input the profile of neutral H density given by Decker and Cheng (1994); in the absence of a better model, we set the N density equal to the H density. Ionization of neutrals via collisions with electrons and solar ultraviolet photons adds both an ion and energy to the magnetosphere. Ionization rates for these processes are taken from Zhang et al. (1991). For the Decker and Cheng neutral profile this gives an ion source of about 4×10^{24} s^{-1}.

When neutrals are ionized by charge exchange, the net plasma density remains the same but the plasma energy changes as the original ion is replaced with an ion at the local rotational energy. If different species are interacting, the charge exchange process can also change the plasma composition. Plasma losses include charge exchange, precipitation into the atmosphere, and losses at the boundaries which occur when ions reach either Neptune's atmosphere or the magnetopause, where the flux tube content is set equal to zero. Precipitation losses are simulated by setting the loss rate to an empirically determined fraction of the strong diffusion loss rate. Additional energy gain or loss occurs via coulomb collisions, which cause energy to move from hotter to cooler species (Spitzer 1962).

Initially we varied the diffusion coefficient D_0 only; the temperatures given by the model were too high and the decrease in NL^2 observed inside L=4 was not reproduced. Two more parameters were varied to bring the model results more in line with observations. We added losses at 1/3 the strong diffusion rate and reduced the rotation speed to 1/2 the corotation speed outside L=13. Figure 22 shows the results of the calculation using the above parameters. The four panels show the NL^2 profile for H^+ and N^+, the temperature profiles for H^+ and N^+, and the model results. A plasma transport rate of $D_0 = 10^{-8} L^3 R_N^2$ s^{-1} is required to fit the data. This gives reasonable agreement with the NL^2 profiles outside L=5. A precipitation loss time which is 1/3 the strong diffusion limit gives a rough approximation of the NL^2 decrease inside L=5. If precipitation at this rate is the operative loss mechanism a method of scattering these ions must be identified. Another possible way to create the decrease in NL^2 is, if the neutral density increases near Neptune, to have charge exchange remove a large fraction of the hot, inward diffusing plasma and replace it with plasma at the local rotational energy. Because this energy, especially for H^+, is well below the instrument threshold of 10 eV, this new plasma would not be observed and would mimic a plasma loss in the observations. A drawback of this mechanism is that a larger difference between the H^+ and N^+ NL^2 profiles might be expected; because the rotation energy of N^+ is 14 times that of H^+, the H^+ would be lost from the instrumental energy range before the N^+, producing a difference in the profiles.

The increase in H^+ temperature outside L=8 could not be reproduced by the model used here. Suggestions that this could result from local mass-loading in this region, so that the energy increase is due to the increase in the corotation energy with L shell (Richardson et al. 1991; Zhang et al. 1991), have proven wrong. A transport rate small enough for charge exchange to provide the observed temperature increase gives too large a total plasma density. This increase in H^+ temperature is not yet understood.

Without assuming a deviation from corotation in the outer magnetosphere, the ion temperatures derived from the Decker and Cheng (1994) source are

such as the magnetopause distance, but for all the outer planets dramatic changes in the plasma character occur between 4 and 6 planetary radii, so use of this scaling seemed appropriate.

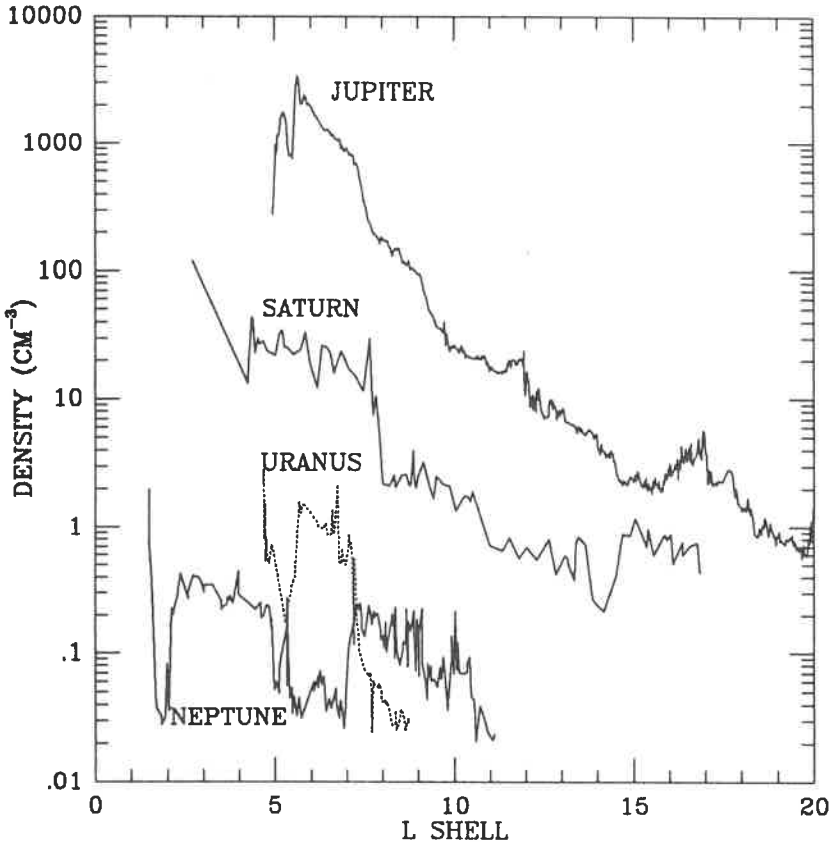

Figure 23. A comparison of plasma number densities at the four outer planets as a function of L shell.

Figure 23 shows the total plasma number density at the four outer planets. Jupiter's magnetosphere contains the highest plasma densities, followed by those of Saturn, Uranus, and then Neptune, although outside L=7 Neptune's magnetospheric densities are larger than those at Uranus. As discussed earlier, a more appropriate quantity to compare is the plasma flux tube content, NL^2, which is shown in Fig. 24. The basic ordering remains the same, but we can now compare the plasma sources. Jupiter's magnetospheric plasma is clearly dominated by a single moon, Io, located at L=5.9 corresponding to the peak in NL^2. Neptune's magnetospheric plasma is also dominated by a single moon, Triton. The NL^2 profile at Saturn is relatively flat; the source of plasma in the

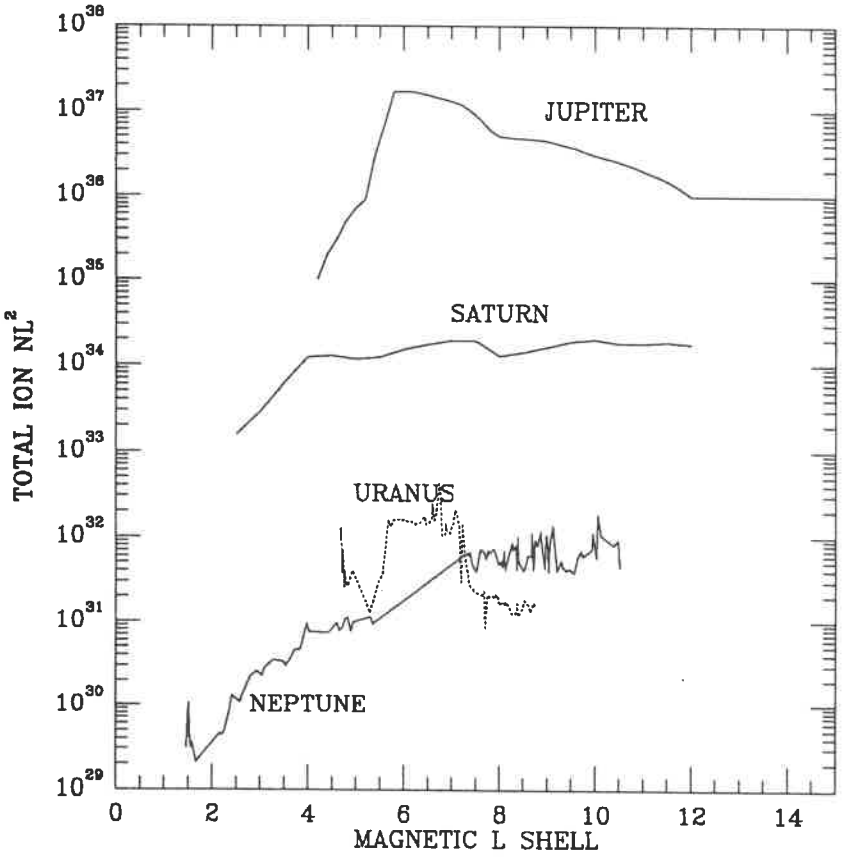

Figure 24. A comparison of flux tube content, NL^2, at the four outer planets as a function of L shell (Voyager 1 at Jupiter, Voyager 2 at Uranus and Neptune, and a combined Voyager 1 and 2 data set at Saturn).

region considered is a large neutral cloud formed from the small icy moons and rings surrounding this planet. The large moon Titan seems to have little effect on the inner magnetosphere of Saturn. Uranus has five very dark moons which apparently inject little plasma into the magnetosphere; no evidence of heavy ions was observed by either the PLS or LECP instruments. The dark surfaces may be indicative of a tar-like surface from which sputtering is difficult. Neptune has several similar small moons, with Proteus large enough to rate consideration as a possible plasma source. These dark moons are as ineffective at populating Neptune's magnetosphere as they are at populating Uranus'.

The plasma energies of the heavy ions at Jupiter, Saturn, and Neptune are shown in Fig. 25. Uranus is not included because no heavy ions were detected. The plasma energies are normalized in energy by dividing the ion

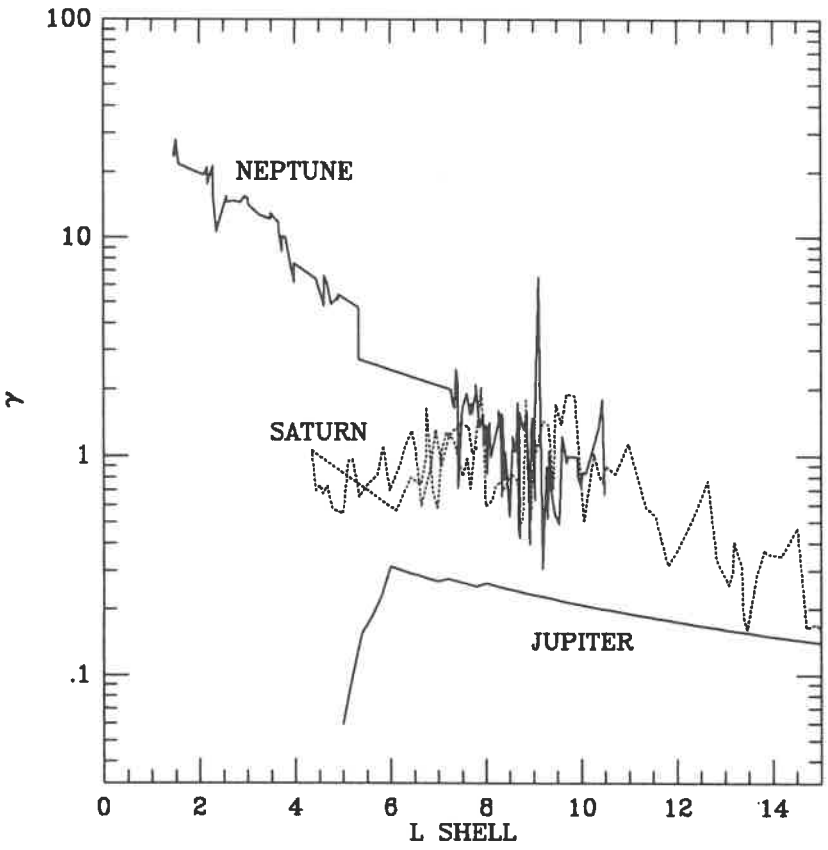

Figure 25. A comparison of plasma energies at the four outer planets as a function of L shell. To compensate for the different planetary rotation rates, we plot the ratio of the heavy ion thermal speed to the corotation speed, which we call γ.

thermal speed by the corotation speed; we call this quantity γ. Thus values of one indicate plasma at its creation energy, values above this indicate the plasma has been heated and values below indicate the plasma has been cooled. The ordering of the planets is reversed in this scheme from that in Fig. 24. The peak at Jupiter is again at Io, but even here radiational cooling is strong enough to reduce γ to less than 1. The value of γ decreases both inside and outside Io, probably due to radiational cooling inside and adiabatic expansion outside. The profile of γ near Saturn is relatively flat from L=4 out to L=11 at a value near 1, indicating plasma throughout this region is picked up locally. Outside L=11 the plasma cools, probably adiabatically. The Neptune profile is near one between L=8 and L=10 and increases inside this. This seems to indicate a plasma source in this region and adiabatic heating inside L=8 as plasma is transported inwards.

What general conclusions can we draw about magnetospheric characteristics from these results? With respect to the magnetospheric plasma, the first important characteristic is the importance of the satellite surfaces in determining whether satellites are plasma sources. At each planet with an active moon and, thus, a constantly recoated surface, that moon provides most of the magnetospheric plasma (Io, Triton). At Saturn, the relatively clean ice surfaces of the inner moons provide the magnetospheric plasma. The only substantial moon/rings which are not major plasma sources are those with very dark surfaces at Uranus and Neptune. The second characteristic is the location of the source. Transport rates are proportional to L to the third or fourth power. Thus for the same source rate, plasma created closer to a planet will build up a larger plasma density. Finally, the magnetic field orientation and strength are important for determining plasma properties. The larger the magnetic field, the bigger the region which is shielded from external effects and the larger the stable inner region where plasma densities can build up. The combination of a spin axis tilted away from the ecliptic and a dipole axis at a large angle from the spin axis allows externally driven (i.e., by the solar wind) convection systems to operate throughout the magnetosphere and limit plasma densities. Such solar wind driven convection may limit the plasma densities at both Uranus and Neptune, whereas internal characteristics limit the plasma density at Jupiter and Saturn.

The Plasma Science experiment on Voyager 2 continues to gather data on the solar wind in the far heliosphere. As with the other fields and particles experiments on Voyager, this investigation has not ended with the magnetosphere of Neptune. Voyager 1 and 2 and Pioneer 10 and 11 continue to operate and send back data from the interplanetary medium. Barring unexpected failures, the Voyagers are expected to operate until at least the year 2015 (Stone and Miner 1991) in their search for the termination of the solar wind, the modulation boundary of galactic cosmic rays, and the beginnings of interstellar space.

Acknowledgments. We thank M. Zhang, A. Eviatar, V. Vasyliunas, G. Siscoe, E. Sittler, Jr., and the two referees for collaboration on this work and/or suggestions on improving the manuscript. This work was supported in part by the National Aeronautics and Space Administration through the Voyager and Neptune Data Analysis Programs.

REFERENCES

Allen, C. W. 1973. *Astrophysical Quantities*, 3rd ed. (London: Athlone Press).

Bagenal, F., and Sullivan, J. D. 1981. Direct plasma measurements in the Io torus and inner magnetosphere of Jupiter. *J. Geophys. Res.* 86:8447–8466.

Bagenal, F., Belcher, J. W., Sittler, E. C., Jr., and Lepping, R. P. 1987. The Uranian bow shock: Voyager 2 inbound observations of a high Mach number shock. *J. Geophys. Res.* 92:8603–8612.

Barbosa, D. D., Kurth, W. S., Cairns, I. H., Gurnett, D. A., and Poynter, R. L. 1990. Electrostatic electron and ion cyclotron harmonic waves in Neptune's magnetosphere. *Geophys. Res. Lett.* 17:1657–1660.

Barnes, A. 1970. Theory of generation of bow-shock-associated hydromagnetic wave in the upstream interplanetary medium. *Cosmic Electrodyn.* 1:90–114.

Behannon, K. W., Goldstein, M. L., Lepping, R. P., Wong, H. K., Mauk, B. H., and Krimigis, S. M. 1985. Low-frequency waves and associated ions downstream of Saturn. *J. Geophys. Res.* 90:10791–10808.

Belcher, J. W., Bridge, H. S., Bagenal, F., Coppi, B., Eviatar, A., Gordon, G. S., Jr., Lazarus, A. J., McNutt, R. L., Jr., Ogilvie, K. W., Richardson, J. D., Siscoe, G. L., Sittler, E. C., Jr., Steinberg, J. T., Sullivan, J. D., Szabo, A., Vasyliunas, V. M., Villanueva, L., and Zhang, M. 1989. Plasma observations near Neptune: Initial results from Voyager 2. *Science* 246:1478–1482.

Bevington, P. R. 1969. *Data Reduction and Error Analysis for the Physical Sciences* (New York: McGraw-Hill).

Brice, N. M., and McDonough, T. R. 1972. Jupiter's radiation belts. *Icarus* 18:206–219.

Bridge, H. S., Belcher, J. W., Butler, R. J., Lazarus, A. J., Mavretic, A. M., Sullivan, J. D., Siscoe, G. L., and Vasyliunas, V. M. 1977. The plasma experiment on the 1977 Voyager mission. *Space Sci. Rev.* 21:259–287.

Broadfoot, A. L., Atreya, S. K., Bertaux, J. L., Blamont, J. E., Dessler, A. J., Donahue, T. M., Forrester, W. T., Hall, D. T., Herbert, F., Holberg, J. B., Hunten, D. M., Krasnopolsky, V. A., Linick, S., Lunine, J. I., McConnell, J. C., Moos, H. W., Sandel, B. R., Schneider, N. M., Shemansky, D. E., Smith, G. R., Strobel, D. F., and Yelle, R. V. 1989. Ultraviolet spectrometer observations of Neptune and Triton. *Science* 246:1459–1466.

Chamberlain, J. W. 1963. Planetary coronae and atmospheric evaporation. *Planet. Space Sci.* 11:901–960.

Cheng, A. F. 1989. Magnetosphere of Neptune: Auroral zone field-aligned potential drops? *Geophys. Res. Lett.* 16:953–956.

Cheng, A. F. 1990. Triton torus and Neptune aurora. *Geophys. Res. Lett.* 17:1669–1672.

Cheng, A. F., Maclennan, C. G., Mauk, B. H., Armstrong T. P., Krimigis S. M., and Lanzerotti, L. J. 1991. Energetic ion phase space densities in Neptune's magnetosphere. *EOS: Trans. AGU* 72:244 (abstract).

Clarke, J. T. 1988. IUE observations of Neptune for H Lyman-α emission. *Geophys. Res. Lett.* 15:701–704.

Connerney, J. E. P., Acuña, M. H., and Ness, N. F. 1991. The magnetic field of Neptune. *J. Geophys. Res.* 96:19023–19042.

Conrath, B., Flasar, F. M., Hanel, R., Kunde, V., Maguire, W., Pearl, J., Pirraglia, J., Samuelson, R., Gierasch, P., Weir, A., Bézard, B., Gautier, D., Cruikshank, D., Horn, L., Springer, R., and Shaffer, W. 1989. Infrared observations of the Neptunian system. *Science* 246:1454–1459.

Coroniti, F. V. 1974. Energetic electrons in Jupiter's magnetosphere. *Astrophys. J. Suppl.* 27:261–281.

Coroniti, F. V., and Kennel, C. F. 1979. Magnetospheric reconnection, substorms, and energetic particle acceleration. In *Particle Acceleration in Planetary Magnetospheres*, eds. J. Arons, C. Max and C. McKee (New York: American Inst. of Physics), pp. 169–178.

Cruikshank, D. P., and Silvaggio, P. M. 1979. Triton: A satellite with an atmosphere. *Astrophys. J.* 233:1016–1020.

Cruikshank, D. P., Brown, R. H., and Clark, R. N. 1984. Nitrogen on Triton. *Icarus* 58:293–305.

Delitsky, M. L., Eviatar, A., and Richardson, J. D. 1989. A predicted Triton plasma torus in Neptune's magnetosphere. *Geophys. Res. Lett.* 16:215–218.

de Pater, I., and Goertz, C. K. 1989. Synchrotron radiation from Neptune: Neptune's magnetic field and electron population. *Geophys. Res. Lett.* 16:97–100.

Decker, R. B., and Cheng, A. F. 1994. A model of Triton's role in Neptune's magnetosphere. *J. Geophys. Res.* 99:19027–19045.

Desch, M. D. 1988. Neptune radio emission: Predictions based on planetary scaling laws. *Geophys. Res. Lett.* 15:114–117.

Dessler, A. J. 1987. The Neptune challenge. *Geophys. Res. Lett.* 14:889.

Dessler, A. J., and Sandel, B. R. 1989. A quiescent magnetosphere for Neptune. *Geophys. Res. Lett.* 16:957–960.

Eviatar, A., McNutt, R. L., Jr., Siscoe, G. L., and Sullivan, J. D. 1983. Heavy ions in the outer Kronian magnetosphere. *J. Geophys. Res.* 88:823–831.

Fairfield, D. H. 1969. Bow shock associated waves observed in the far upstream interplanetary medium. *J. Geophys. Res.* 74:3541–3553.

Fairfield, D. H., and Behannon, K. W. 1976. Bow shock and magnetosheath waves at Mercury. *J. Geophys. Res.* 81:3897–3906.

Fälthammar, C.-G. 1968. Radial diffusion by violation of the third adiabatic invariant. In *Earth's Particles and Fields*, ed. B. M. McCormac (New York: Reinhold), pp. 157–169.

Gary, S. P., Gosling, J. T., and Forslund, D. W. 1981. The electromagnetic ion beam instability upstream of the Earth's bow shock. *J. Geophys. Res.* 86:6691–6698.

Goertz, C. K., and Thomsen, M. F. 1979. Radial diffusion of Io injected plasma. *J. Geophys. Res.* 84:1499–1504.

Gurnett, D. A., Kurth, W. S., Cairns, I. H., and Granroth, L. J. 1990. Whistlers in Neptune's magnetosphere: Evidence of atmospheric lightning. *J. Geophys. Res.* 95:20957–20976.

Hardy, D. A., Hills, H. K., and Freeman, J. W. 1975. A new plasma regime in the distant geomagnetic tail. *Geophys. Res. Lett.* 2:169–172.

Hill, T. W. 1979. Inertial limit on corotation. *J. Geophys. Res.* 84:6554–6558.

Hill, T. W., and Dessler, A. J. 1990. Convection in Neptune's magnetosphere. *Geophys. Res. Lett.* 17:1677–1680.

Hood, L. L. 1983. Radial diffusion in Saturn's radiation belts: A modeling analysis assuming satellite and ring E absorption. *J. Geophys. Res.* 88:808–818.

Hood, L. L. 1985. Radial diffusion in Saturn's radiation belts: A combined analysis of phase space density and satellite microsignature data. *J. Geophys. Res.* 90:6295–6303.

Hood, L. L. 1989*a*. Radial diffusion and losses of energetic protons in the 5 to 12 R_S region of Saturn's magnetosphere. *J. Geophys. Res.* 94:8721–8730.

Hood, L. L. 1989*b*. Radial diffusion in the Uranian radiation belts: Inferences from satellite absorption loss models. *J. Geophys. Res.* 94:15077–15088.

Hoppe, M. M., and Russell, C. T. 1981. On the nature of ULF waves upstream of planetary bow shock. *Adv. Space Res.* 1:322–327.

Ip, W.-H. 1990. On the ionosphere of Triton: An evaluation of the magnetospheric electron precipitation and photoionization effects. *Geophys. Res. Lett.* 17:1713–1716.

Krimigis, S. M., and Armstrong, T. P. 1982. Two-component proton spectra in the inner Saturnian magnetosphere. *Geophys. Res. Lett.* 9:1143–1146.

Krimigis, S. M., Armstrong, T. P., Axford, W. I., Bostrom, C. O., Cheng, A. F., Gloeckler, G., Hamilton, D. C., Keath, E. P., Lanzerotti, L. J., Mauk, B. H., and Van Allen, J. A. 1989. Hot plasma and energetic particles in Neptune's magnetosphere. *Science* 246:1483–1489.

Krimigis, S. M., Mauk, B. H., Cheng, A. F., Keath, E. P., Kane, M., Armstrong, T. P., Gloeckler, G., and Lanzerotti, L. J. 1990. Hot plasma parameters in Neptune's magnetosphere. *Geophys. Res. Lett.* 17:1685–1689.

Kurth, W. S., Barbosa, D. D., Gurnett, D. A., Poynter, R. L. and Cairns, I. H. 1990. Low-frequency radio emissions at Neptune. *Geophys. Res. Lett.* 17:1649–1652.

Lazarus, A. J., and McNutt, R. L., Jr. 1983. Low-energy plasma ion observations in Saturn's magnetosphere. *J. Geophys. Res.* 88:8831–8846.

Lepping, R. P., Burlaga, L. F., Lazarus, A. J., Vasyliunas, V. M., Szabo, A., Steinberg, J. T., Ness, N. F., and Krimigis, S. M. 1992. Neptune's polar cusp region: Observations and magnetic field analysis. *J. Geophys. Res.* 97:8135–8144.

Leroy, M. M. 1983. Structure of perpendicular shocks in collisionless plasma. *Phys. Fluids* 26:2742–2753.

Lindal, G. F., Lyons, J. R., Sweetnam, D. N., Eshleman, V. R., Hinson, D. P., and Tyler, G. L. 1990. The atmosphere of Neptune: Results of radio occultation measurements with the Voyager 2 spacecraft. *Geophys. Res. Lett.* 17:1733–1736.

Lyons, J. R., Yung, Y. L., and Allen, M. 1992. Solar control of the upper atmosphere of Triton. *Science* 256:204–206.

Majeed, T., McConnell, J. C., Strobel, D. F., and Summers, M. E. 1990. The ionosphere of Triton. *Geophys. Res. Lett.* 17:1721–1724.

Mauk, B. H., Kane, M., Keath, E. P., Cheng, A. F., Krimigis, S. M., Armstrong, T. P., and Ness, N. F. 1990. Energetic charged particle angular distributions near ($r < 2\ R_n$) and over the pole of Neptune. *Geophys. Res. Lett.* 17:1701–1704.

McConnell, J. C., Parkinson, C. D., Ben-Jaffel, L., Emerich, C., Prangöée, R., and Vidal-Madjar, A. 1989. H Lyman-α emission at Neptune: Voyager prediction. *Astron. Astrophys.* 225:L9–L12.

McNutt, R. L., Jr., Belcher, J. W., and Bridge, H. S. 1981. Positive ion observations in the middle magnetosphere of Jupiter. *J. Geophys. Res.* 86:8319–8342.

Menietti, J. D., Tsintikidis, D., Gurnett, D. A., and Curran, D. B. 1991. Modeling of whistler ray paths in the magnetosphere of Neptune. *J. Geophys. Res.* 96:19117–19122.

Million, M. A., and Goertz, C. K. 1988. Prediction of radio frequency power generation of Neptune's magnetosphere from generalized radiometric Bode's law. *Geophys. Res. Lett.* 15:111–113.

Ness, N. F., Acuña, M. H., Burlaga, L. F., Connerney, J. E. P., Lepping, R. P., and Neubauer, F. M. 1989. Magnetic fields at Neptune. *Science* 246:1473–1478.

Ness, N. F., Connerney, J. E. P., Lepping, R. P., Schulz, M., and Voigt, G.-H. 1991. The magnetic field and magnetospheric configuration of Uranus. In *Uranus*, eds. J. T. Bergstralh, E. D. Miner and M. S. Matthews (Tucson: Univ. of Arizona Press), pp. 739–779.

Northrup, T. 1963. *The Adiabatic Motion of Charged Particles* (New York: Interscience).

Paschmann, G., Haerendel, G., Sckopke, N., Rosenbauer, H., and Hedgecock, P. C. 1976. Plasma and magnetic field characteristics of the distant polar cusp near local noon: The entry layer. *J. Geophys. Res.* 81:2883–2899.

Paschmann, G., Sckopke, N., Bame, S. J., and Gosling, J. T. 1982. Observations of gyrating ions in the foot of the nearly perpendicular bow shock. *Geophys. Res. Lett.* 9:881–884.

Pontius, D. H., and Hill, T. W. 1982. Departure from corotation of the Io plasma torus: Local plasma production. *Geophys. Res. Lett.* 9:1321–1324.

Richardson, J. D. 1986. Thermal ions at Saturn: Plasma parameters and implications. *J. Geophys. Res.* 91:1381–1389.

Richardson, J. D. 1994. A quantitative model of plasma in Neptune's magnetosphere. *Geophys. Rev. Lett.* 20:1467–1470.

Richardson, J. D., and Siscoe, G. L. 1983. The problem of cooling the cold Io torus. *J. Geophys. Res.* 88:2001–2009.

Richardson, J. D., and McNutt, R. L., Jr. 1990. Low-energy plasma in Neptune's magnetosphere. *Geophys. Res. Lett.* 17:1689–1692.

Richardson, J. D., and Sittler, E. C., Jr. 1990. A plasma density model for Saturn based on Voyager observations. *J. Geophys. Res.* 95:12019–12031.

Richardson, J. D., Eviatar, A., and Delitsky, M. L. 1990. The Triton torus revisited. *Geophys. Res. Lett.* 17:1673–1676.

Richardson, J. D., Belcher, J. W., Zhang, M., and McNutt, R. L., Jr. 1991. Low-energy ions near Neptune. *J. Geophys. Res.* 96:18993–19011.

Richardson, J. D., Stahara, S. S., Siscoe, G. L., Spreiter, J. R., and Szabo, A. 1994. The magnetosheath of Neptune: Models and observations. *J. Geophys. Res.* 99:14789–14798.

Romani, P. N., de Pater, I., and Atreya, S. K. 1989. Neptune's deep atmosphere revealed. *Geophys. Res. Lett.* 16:933–936.

Rosenbauer, H., Grunwaldt, H., Montgomery, M. D., Paschmann, G., and Sckopke, N. 1975. Heos 2 plasma observations in the distant polar magnetosphere: The plasma mantle. *J. Geophys. Res.* 80:2723–2737.

Rossi, B., and Olbert, S. 1970. *Introduction to the Physics of Space* (New York: McGraw-Hill).

Russell, C. T. 1985. Planetary bow shocks. In *Collisionless Shocks in the Heliosphere: Review of Current Research*, eds. B. T. Tsurutani and R. G. Stone (Washington, D. C.: American Geophysical Union), pp. 109–130.

Russell, C. T., Lepping, R. P., and Smith, C. W. 1990. Upstream waves at Uranus. *J. Geophys. Res.* 95:2273–2280.

Sawyer, C., Warwick, J. W., and Romig, J. H. 1990. Smooth radio emission and a new emission at Neptune. *Geophys. Res. Lett.* 17:1645–1648.

Scarf, F. L., Fredricks, R. W., Frank, L. A., Russell, C. T., Coleman, P. J., Jr., and Neugebauer, M. 1970. Direct correlations of large-amplitude waves with suprathermal protons in the upstream solar wind. *J. Geophys. Res.* 75:7316–7322.

Schulz, M., and Lanzerotti, L. J. 1974. *Particle Diffusion in the Radiation Belts* (New York: Springer-Verlag).

Schwartz, S. J. 1985. Solar wind and the Earth's bow shock. In *Solar System Magnetic Fields*, ed. E. R. Priest (Dordrecht: Kluwer), pp. 25–36.

Schwartz, S. J., Thomsen, M. F., and Gosling, J. T. 1983. Ions upstream of the Earth's bow shock: A theoretical comparison of alternative source populations. *J. Geophys. Res.* 88:2039–2047.

Scudder, J. D., Mangeney, A., Lacombe, C., Harvey, C. C., Aggson, T. L., Anderson, R. R., Gosling, J. T., Paschmann, G., and Russell, C. T. 1986*a*. The resolved layer of a collisionless, high β supercritical, quasi-perpendicular shock wave, 1: Rankine-Hugoniot geometry, currents and stationarity. *J. Geophys. Res.* 91:11019–11052.

Scudder, J. D., Mangeney, A., Lacombe, C., Harvey, C. C., and Aggson, T. L. 1986*b*. The resolved layer of a collisionless, high β supercritical, quasi-perpendicular shock wave, 2: Dissipative fluid electrodynamics. *J. Geophys. Res.* 91:11053–11074.

Scudder, J. D., Mangeney, A., Lacombe, C., Harvey, C. C., Wu, C. S., and Anderson, R. R. 1986*c*. The resolved layer of a collisionless, high β supercritical, quasi-perpendicular shock wave, 3: Vlasov electrodynamics. *J. Geophys. Res.* 91:11075–11098.

Selesnick, R. S. 1990. Plasma convection in Neptune's magnetosphere. *Geophys. Res. Lett.* 17:1681–1684.

Selesnick, R. S. 1992. Magnetic field models from energetic particle data at Neptune. *J. Geophys. Res.* 97:10857–10864.

Selesnick, R. S., and McNutt, R. L., Jr. 1987. Voyager 2 plasma ion observations in the magnetosphere of Uranus. *J. Geophys. Res.* 92:15249–15262.

Simpson, J. A., Bastian, T. S., Chenette, D. L., McKibben, R. B., and Pyle, K. R. 1980. The trapped radiations at Saturn and their absorption by satellites and rings. *J. Geophys. Res.* 85:5731–5762.

Siscoe, G. L. 1988. The magnetic boundary. In *Physics of Space Plasmas*, eds. T. Chang, G. B. Crew and J. R. Jasperse (Cambridge, Mass.: Scientific), pp. 3–78.

Siscoe, G. L., and Sanchez, E. 1987. An MHD model for the complete open magnetotail boundary. *J. Geophys. Res.* 92:7405–7412.

Sittler, E. C., and Scudder, J. D. 1980. An empirical polytrope law for solar wind thermal electrons between 0.45 and 4.76 AU: Voyager 2 and Mariner 10. *J. Geophys. Res.* 85:5131–5137.

Sittler, E. C., Jr., Ogilvie, K. W., and Selesnick, R. S. 1987. Survey of electrons in the Uranian magnetosphere: Voyager 2 observations. *J. Geophys. Res.* 92:15263–15281.

Slavin, J. A., Holzer, R. E., Spreiter, J. R., Stahara, S. S., and Chaussee, D. S. 1983. Solar wind flow about the terrestrial planets, 2, Comparison with gas dynamic theory and implications for solar-planetary interactions. *J. Geophys. Res.* 88:19–35.

Slavin, J. A., Smith, E. J., Spreiter, J. R., and Stahara, S. S. 1985. Solar wind flow about the outer planets: Gas dynamic modeling of the Jupiter and Saturn bow shocks. *J. Geophys. Res.* 90:6275-6286.

Smith, B. A., Soderblom, L. A., Banfield, D., Barnet, C., Basilevsky, A. T., Beebe, R. F., Bollinger, K., Boyce, J. M., Brahic, A., Briggs, G. A., Brown, R. H., Chyba, C., Collins, S. A., Colvin, T., Cook, A. F., II, Crisp, D., Croft, S. K., Cruikshank, D., Cuzzi, J., N., Danielson, G. E., Davies, M. E., De Jong, E., Dones, L., Godfrey, D., Goguen, M., Grenier, I., Haemmerle, V. R., Hammel, H., Hansen, C. J., Helfenstein, C. P., Howell, C., Hunt, G. E., Ingersoll, A. P., Johnson, T. V., Kargel, J., Kirk, R., Kuehn, D. I., Limaye, S., Masursky, H., McEwen, A., Morrison, D., Owen, T., Pollack, J. B., Porco, C. C., Rages, K., Rogers, P., Rudy, D., Sagan, C., Schwartz, J., Shoemaker, E. M., Showalter, M., Sicardy, B., Simonelli, D., Spencer, J., Sromovsky, L. A., Stoker, C., Strom, R. G., Suomi, V. E., Synnott, S. P., Terrile, R. J., Thomas, P., Thompson, W. R., Verbiscer, A., and Veverka, J. 1989. Voyager 2 at Neptune: Imaging science results. *Science* 246:1422–1449.

Smith, G. J., Tsurutani, B. T., Chenette, D. L., Conlon, T. F., and Simpson, J. A. 1976. Jovian electron bursts: Correlation with the interplanetary field direction and hydromagnetic waves. *J. Geophys. Res.* 81:65–72.

Spitzer, L., Jr. 1962. *Physics of Fully Ionized Gases*, 2nd ed. (New York: Interscience).

Spreiter, J. R., Summers, A. L., and Alksne, A. Y. 1966. Hydromagnetic flow around the magnetosphere. *Planet. Space Sci.* 14:223–253.

Spreiter, J. R., and Stahara, S. S. 1980*a*. A new predictive model for determining solar wind terrestrial planet interactions. *J. Geophys. Res.* 85:6769–6777.

Spreiter, J. R., and Stahara, S. S. 1980*b*. Solar wind flow past Venus: Theory and comparisons. *J. Geophys. Res.* 85:7715–7738.

Spreiter, J. R., and Stahara, S. S. 1985. Magnetohydrodynamic and gasdynamic theories for planetary bow waves. In *Collisionless Shocks in the Heliosphere, Review of Current Research*, eds. B. T. Tsurutani and R. G. Stone (Washington, D. C.: American Geophysical Union), pp. 85–107.

Stahara, S. S., Klenke, D., Trudinger, B. C., and Spreiter, J. R. 1980. *Application Of Advanced Computational Procedures For Modeling Solar-Wind Interactions With Venus: Theory And Computer Code.* NASA CR-3267.

Stahara, S. S., Rachiele, R. R., Spreiter, J. R., and Slavin, J. A. 1989. A three dimensional gasdynamic model for solar wind flow past nonaxisymmetric magnetospheres: Application to Jupiter and Saturn. *J. Geophys. Res.* 94:13353–13365.

Stone, E. C., and Miner, E. D. 1989. The Voyager 2 encounter with the Neptunian system. *Science* 246:1417–1421.

Stone, E. C., and Miner, E. D. 1991. The Voyager encounter with Neptune. *J. Geophys. Res.* 96:18903–18906.

Stone, E. C., Cummings, A. C., Looper, M. D., Selesnick, R. S., Lal, N., McDonald, F. B., Trainor, J. H. and Chenette, D. L. 1989. Energetic charged particles in the magnetosphere of Neptune. *Science* 246:1498–1494.

Strobel, D. F., and Atreya, S. K. 1983. Ionosphere. In *Physics of the Jovian Magnetosphere*, ed. A. J. Dessler (New York: Cambridge Univ. Press), pp. 51–67.

Summers, M. E., and Strobel, D. F. 1991. Triton's atmosphere: A source of N and H for Neptune's magnetosphere. *Geophys. Res. Lett.* 18:2309–2312.

Szabo, A. 1994. An improved solution to the "Rankine-Hugoniot" problem. *J. Geophys. Res.* 99:14737–14746.

Szabo, A., and Lepping, R. P. 1995. Neptune inbound bow shock. *J. Geophys. Res.*, 100:1723–1730.

Szabo, A., Siscoe, G. L., Lazarus, A. J., McNutt, R. L., Jr., Lepping, R. P., and Ness, N. F. 1991. Magnetopause and cusp observations at Neptune. *J. Geophys. Res.* 96:19149–19153.

Tsurutani, B. T., and Stone, R. G., eds. 1985. *Collisionless Shocks in the Heliosphere: Reviews of Current Research* (Washington, D. C.: American Geophysical Union).

Tyler, G. L., Sweetnam, D. N., Anderson, J. D., Borutzki, S. E., Campbell, J. K., Eshleman, V. R., Gresh, D. L., Gurrola, E. M., Hinson, D. P., Kawashima, N., Kursinski, E. R., Levy, G. S., Lindal, G. F., Lyons, J. R., Marouf, E. A., Rosen, P. A., Simpson, R. A., and Wood, G. E. 1989. Voyager radio science observations of Neptune and Triton. *Science* 246:1466–1473.

Van Allen, J. A. 1983. Absorption of energetic protons by Saturn's ring G. *J. Geophys. Res.* 88:6911–6918.

Van Allen, J. A., Thomsen, M. F., Randall, B. A., Rairden, R. L., and Grosskreutz, C. L. 1980. Saturn's magnetosphere, rings and inner satellites. *Science* 207:415–421.

Vasyliunas, V. M. 1971. Deep space plasma measurements. *Methods Exper. Phys.* 9B:49–88.

Vasyliunas, V. M. 1983. Plasma distribution and flow. In *Physics of the Jovian Magnetosphere*, ed. A. J. Dessler (New York: Cambridge Univ. Press), pp. 395–453.

Vinas, A. F., and Scudder, J. D. 1986. Fast and optimal solution to the Rankine-Hugoniot problem. *J. Geophys. Res.* 91:39–58.

Warwick, J. W., Evans, D. R., Peltzer, G. R., Peltzer, R. G., Romig, J. H., Sawyer, C. B., Riddle, A. C., Schweitzer, A. E., Desch, M. D., Kaiser, M. L., Farrell, W. M., Carr, T. D., de Pater, I., Staelin, D. H., Gulkis, S., Poynter, R. L., Boischot, A.,

Genova, F., Leblanc, Y., Lecacheux, A., Pedersen, B. M., and Zarka, P. 1989. Voyager planetary radio astronomy at Neptune. *Science* 246:1498–1501.
Yelle, R. V., Doose, L. R., Tomasko, M. G., and Strobel, D. F. 1987. Analysis of Raman scattered Ly-α emissions from the atmosphere of Uranus. *Geophys. Res. Lett.* 14:483–486.
Yung, Y. L., and Lyons, J. R. 1990. Triton: Topside ionosphere and nitrogen escape. *Geophys. Res. Lett.* 17:1717–1720.
Zhang, M., Vasyliunas, V. M., Siscoe, G. L., Lepping, R. P., and Ness, N. F. 1990. Evidence for a diurnally rocking plasma mantle at Neptune. *Geophys. Res. Lett.* 17:2285–2288.
Zhang, M., Belcher, J. W., Richardson, J. D., and Smith, C. W. 1991. Alfvén waves and associated energetic ions downstream from Uranus. *J. Geophys. Res.* 96:1647–1660.
Zhang, M., Belcher, J. W., Richardson, J. D., Vasyliunas, V. M., Lepping, R. P., Ness, N. F., and Smith, C. W. 1991. Low-frequency waves in the solar wind near Neptune. *Geophys. Res. Lett.* 18:1071–1074.
Zhang, M., Richardson, J. D., and Sittler, E. C., Jr. 1991. Voyager 2 electron observations in the magnetosphere of Neptune. *J. Geophys. Res.* 96:19085–19100.

RADIO EMISSIONS FROM NEPTUNE

PHILIPPE ZARKA, BENT M. PEDERSEN and ALAIN LECACHEUX
Observatoire de Paris

MICHAEL L. KAISER, MICHAEL D. DESCH and
WILLIAM M. FARRELL
NASA Goddard Space Flight Center

and

WILLIAM S. KURTH
The University of Iowa

The 1989 Voyager 2 rapid flyby demonstrated that Neptune is a weak source of nonthermal radio emissions, counting no less than five distinct components. These include one of the most impulsive narrowbanded emissions ("bursty" component) ever detected from a radio planet and a slowly varying ("smooth") component with very intricate polarization features, which constitute Neptune's main auroral emissions. Their analysis and interpretation allowed to derive an accurate estimate of Neptune's rotation period (16h 06m 30s±24s). The ubiquitous nonthermal "continuum" radiation, which has now been observed at all outer planetary magnetospheres, is thoroughly discussed. We review the physical properties of all these emissions, including their propagation mode, source location and beaming pattern, and discuss their generation mechanisms in the context of comparative radio planetology. In particular, the striking similarities existing between nearly all their radio components make Neptune and Uranus appear as "radio twins." Constraints on the plasma content in Neptune's auroral regions are drawn from the characteristics of the bursts and their interpretation. Finally, we discuss a possible lightning activity in Neptune's atmosphere and estimate an upper limit for the intensity of the associated radio emissions.

I. INTRODUCTION

A. Discovery of Neptunian Radio Emissions

The first recognition of radio activity from Neptune occurred at 0610 SCET (spacecraft event time) on 17 August 1989 or DOY (day of year) 229 1989, about 8 days prior to closest approach (CA) (Warwick et al. 1989). The observations consisted of a cluster of narrowbanded, short duration bursts that extended from 635 to 865 kHz. Figure 1 is a radio spectrogram showing this discovery episode. Note that the individual events are "spiky" in appearance.

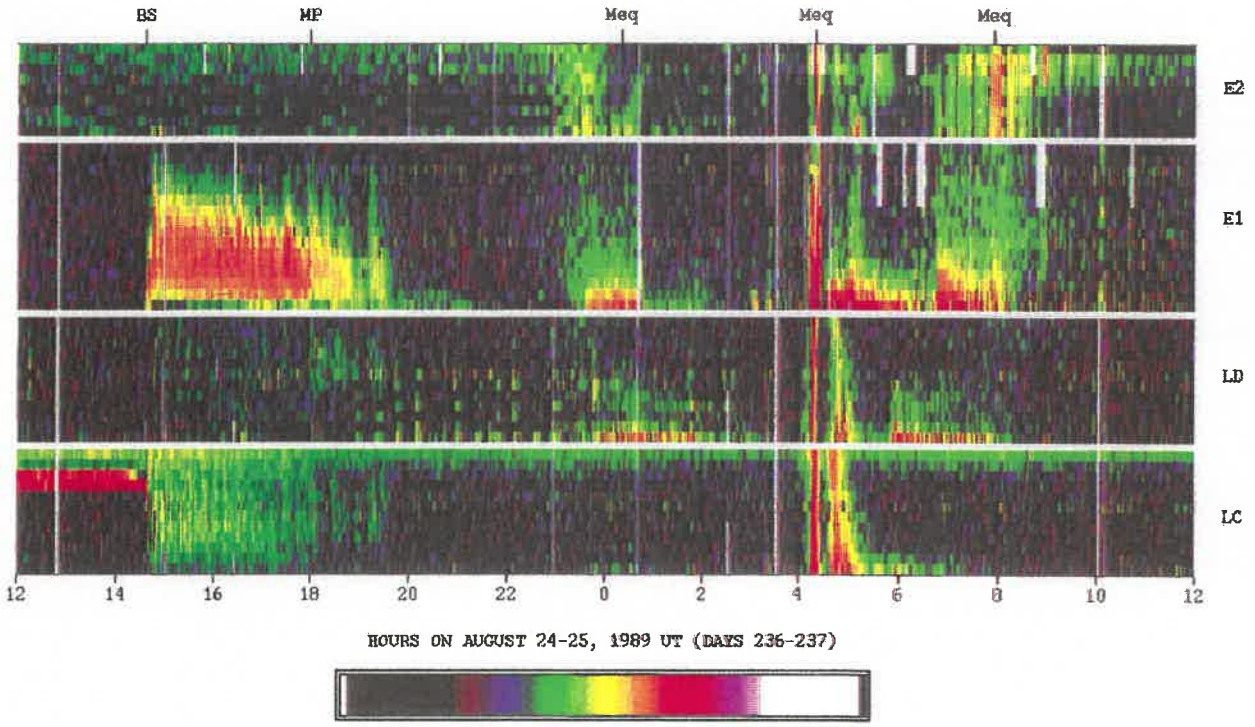

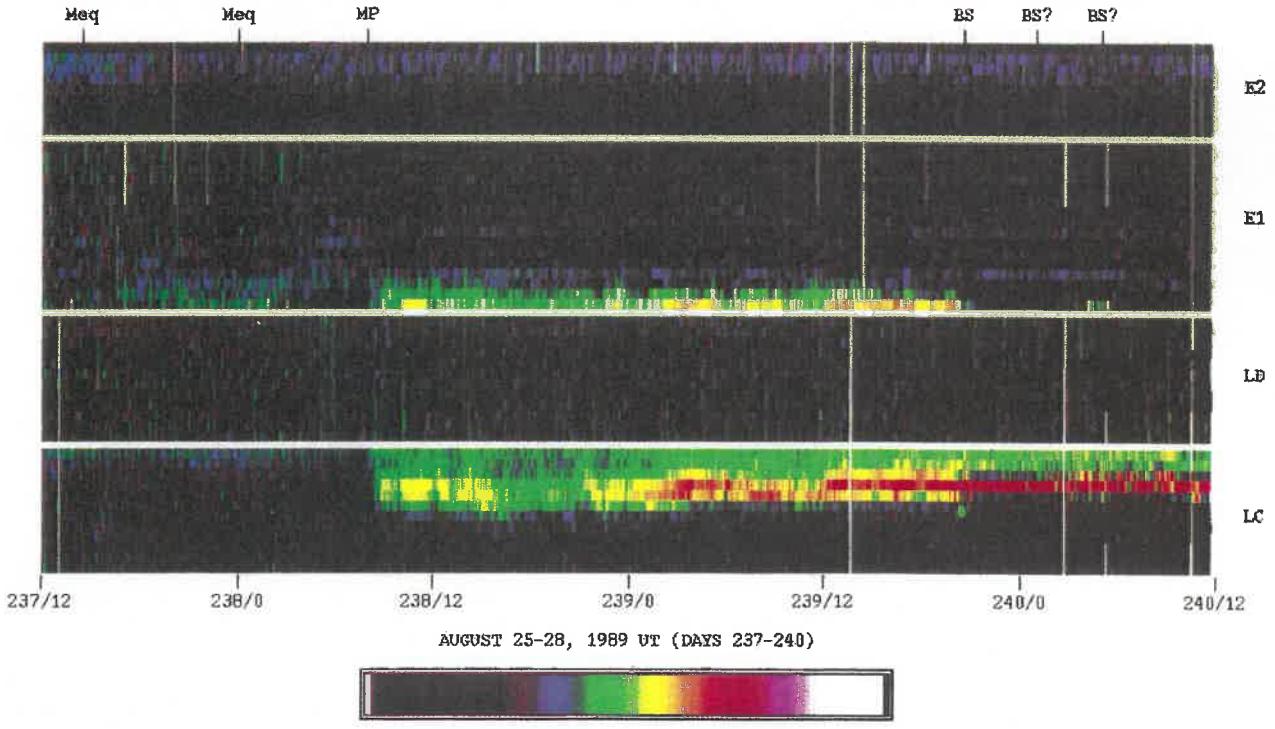

Plates 6 and 7. Color spectrograms showing an overview of the Neptune encounter from the PLS perspective. From top to bottom are the high-energy electrons (140–2480 eV), low-energy electrons (10–140 eV), ions in the sunward-looking *C* cup (10–1850 eV), and ions in the azimuthally looking *D* cup (10–1850 eV). The energy scales are approximately logarithmic. The highest-energy channels are contaminated by noise and are not shown. See the Chapter by Richardson et al.